*Clays and Clay Minerals*, Vol. 56, No. 6, 730–750, 2008.

# CLAY MINERALS IN BASALT-HAWAIITE ROCKS FROM MURUROA ATOLL (FRENCH POLYNESIA). II. PETROGRAPHY AND GEOCHEMISTRY

ALAIN MEUNIER*, ANTOINE MAS, DANIEL BEAUFORT, PATRICIA PATRIER, AND PATRICK DUDOIGNON

University of Poitiers, HydrASA INSU-CNRS, 40 avenue Recteur Pineau, 86022 Poitiers Cedex, France

**Abstract**—The clay minerals formed in chilled margins and massive crystallized inner parts of three basalt-hawaiite bodies of Mururoa Atoll (French Polynesia) exhibit contrasting textures. Glass alteration textures are observed around fractures crosscutting the quenched margins: Fe-rich clays grow inward into the glass (retreating surface) while Mg-rich clays grow outward (open space). The textures of clay deposits filling the diktytaxitic voids (mesostasis) in the massive inner parts of the three volcanic bodies are different: unoriented clay matrix with embedded euhedral apatite and pyroxene microcrysts (submarine flow); pallisadic clays coating the void walls and the crystal surfaces of apatite and K-feldspar microcrysts (subaerial flow); and clay muffs covering all the apatite needles, with the central part of the void remaining empty (dike). The unoriented texture could result from the alteration of a glass precursor concomitant with the olivine phenocrysts (clay pseudomorphs). However, such an alteration implies important chemical transfers which are not observed. The pallisadic and muff textures form through heterogeneous nucleation on the solid surfaces and crystal growth from a saline solution. No glass precursor existed. As the center of the diktytaxitic voids in the dike is empty, the residual liquid was probably boiling. The amounts of light rare earth elements (*LREE*), Sr, and the most incompatible elements are greater in clays from diktytaxitic voids relative to the amounts formed in the altered glass of the chilled margins. Thus, diktytaxitic clays formed from a residual liquid which gave either an evolved glass or a saline solution after cooling (fractionation process). The $\delta^{18}O$ variation *vs.* loss on ignition (LOI) indicates that sea water was involved either in rock alteration or magma contamination. This is confirmed by the $^{87}Rb/^{86}Sr$ ratio of bulk rocks and clay fractions from the quenched and massive inner parts of the three volcanic bodies which do not fit with the 11.5 Ma isochron indicating that the Rb-Sr system was not closed at any stage during the magmatic history.

**Key Words**—Basalt Alteration, Diktytaxitic Void, French Polynesia, Isotopes, Mesostasis Texture, Mururoa Atoll.

## INTRODUCTION

Basaltic flows or dikes generally exhibit a crystallized inner part surrounded by quenched margins at the interface with their environment (cold host rocks, sea or fresh water, atmosphere). These quenched margins are not or are partially crystallized as shown by the presence of a basaltic glass in which the plagioclase microliths and pyroxene microcrysts are scattered. Both the inner crystallized body and the quenched margins contain more or less spherical vesicles or microvesicles which formed during the degassing event of the magma. The rounded shape results from a gas-liquid interface equilibrium. Most often, these vesicles are rimmed by clay minerals and sealed by zeolites (amygdales). The inner part of the volcanic body is almost entirely crystalline giving typical textures in which the phenocrysts are scattered in a microcrystalline matrix. In basalt-hawaiite rocks, plagioclase and pyroxenes form phenocrysts and matrix microliths or microcrysts while olivine is mainly observed as phenocrysts. Interstitial angular free spaces bordered by these crystals are common in the matrix, *i.e.* the diktytaxitic voids (Walker, 1989). They result from a filtering process of liquids and gas during the late cooling stage when the magma has almost completely crystallized (Anderson *et al.*, 1984).

The diktytaxitic voids are frequently filled by an optically amorphous mesostasis which is considered to be glassy. This is the case when the mesostasis is particularly dark (black mesostasis): (1) tachylite-type glass with numerous opaque microcrysts (McPhie *et al.*, 1993); (2) rhyolitic glass (Anderson *et al.*, 1984; Bates and Jackson, 1987; Destrigneville *et al.*, 1991; McPhie *et al.*, 1993; Goff, 1996). Glass is considered to be the end product of the magma crystallization sequence (Ryan and Sammis, 1981; Anderson *et al.*, 1984), or of the quenching caused by the percolation of water through fissure networks opened during the cooling of the lava (Jaeger, 1968; DeGraff and Aydin, 1993; Brilha, 1997). However, the mesostasis is not always black but sometimes green, in which case it is not glassy but mostly composed of clay minerals.

Clays are classically considered to be the alteration products of a pre-existing glass, *i.e.* the products of mineral reactions triggered by the interaction of the less stable solid component of a lava body with infiltrated

* E-mail address of corresponding author:
alain.meunier@univ-poitiers.fr
DOI: 10.1346/CCMN.2008.0560612

aqueous fluids (Andrews, 1980; Dudoignon *et al.*, 1997; Schiffman and Day, 1999; Alt, 1999). In such conditions, glass and olivine are the best candidates for the development of clay pseudomorphs in basaltic rocks. Do the clay minerals represent secondary products replacing the more reactive solid part of the basaltic rocks or is another process involved which leads to their direct precipitation from the resident fluids trapped in the basaltic rocks at the moment of their total solidification?

To address this question requires a detailed study of the clay assemblages crystallized during the cooling history of different types of basaltic bodies related to a same magmatic chamber. In the present study, three basalt-hawaiite bodies from Mururoa Atoll (French Polynesia) were investigated. Bodies far from hydrothermal zones and from any sea-water interface were selected: subaerial and submarine flows and a dike. All have chilled margins and massive inner parts.

This work represents the second part of a study which attempts to depict both the nature and the origin of the clay minerals in the basalt-hawaiite rocks from the Mururoa Atoll. The detailed characterization of the clay parageneses are treated in the first part (Mas *et al.*, 2008). The aim of the present work was to investigate the origin of the clay minerals forming the mesostasis in the diktytaxitic voids and the deposits in the microvesicles. Two key questions are: (1) Do clay minerals in diktytaxitic voids and microvesicles result necessarily from the alteration of a pre-existing glass triggered by a fluid invasion? (2) What is the origin of the fluid from which the clay minerals crystallized? The first question is addressed through a comparison of the textures of clay deposits in fractures crosscutting the glassy margins on one hand and diktytaxitic voids on the other. The second question is addressed through study of the geochemical and isotopic properties of the clay fraction extracted from the quenched margins and the massive inner crystallized parts of the three volcanic bodies.

## ANALYTICAL METHODS

The mineralogical composition of clay deposits in veins, vesicles, and mesostasis of the quenched margins and the massive inner parts of the subaerial and submarine flows and of the dike are summarized (Table 1; see Mas *et al.*, 2008, for details). Sections of rocks and areas of thin sections were selected for a detailed petrographic study of the clay deposits in fractures, vesicles, and diktytaxitic voids. Scanning electron microscopy (SEM) was performed using a JEOL 6400 device equipped with a KEVEX energy dispersive X-ray fluorescence analysis system (Si-Li diode – EDS) both in the secondary (SE) and backscattered electron (BSE) modes on small slabs of rocks (several $mm^3$) and petrographic thin sections coated with carbon. The analytical conditions for quantitative analyses were: accelerating voltage 15 kV, counting time 100 s, beam intensity $6 \times 10^{-10}$ A. The system was calibrated using mineral standards. The matrix corrections were calculated using a ZAF correction program (Reed, 1993).

Electron microprobe analyses were performed using a CAMECA SX50 electron microprobe equipped with wavelength dispersive spectrometers (Camparis microanalysis service of Paris VI University). The analytical conditions were: 4 nA, 15 kV, spot size 4 μm, counting time 10 s per element. The quantitative analyses were obtained by comparison with natural and synthetic silicate standards ($MnTiO_3$, hematite, albite, orthoclase, and diopside) using a CAMECA PAP matrix correction (Pouchou and Pichoir, 1984). The amounts of Fe in the glass and phyllosilicates were arbitrarily calculated as FeO% and $Fe_2O_3$%, respectively.

Chemical analyses of the bulk rocks and of the clay fractions were performed using <5 μm and <0.2 μm powders, respectively, at the Service d'Analyse des Roches et des Minéraux (SARM), Nancy, France (www.crpg.cnrs-nancy.fr/SARM/). Major elements and rare earth elements (*REE*) were analyzed using atomic absorption spectrometry (AA), inductively coupled plasma atomic emission spectroscopy, and inductively coupled plasma mass spectrometry. The amounts of *REE* were normalized to the primitive mantle composition (Sun and McDonough, 1989). Stable and radiogenic isotopes (O, Sr, Rb) were analyzed using mass spectrometry. The loss on ignition (LOI) was measured using a Netzsch apparatus (STA 409 EP) for simultaneous thermal analyses. The amounts of Fe for bulk rocks were arbitrarily calculated as $Fe_2O_3$%.

## RESULTS

Vesicles and veins occurred in the massive inner parts of the submarine flow and of the dike but not in the

Table 1. Composition of the clay mineral assemblages from the chilled margins and the massive crystallized inner parts of the subaerial and submarine flows and the dike (Mururoa Atoll, French Polynesia).

| Volcanic body | Chilled margins | Massive parts |
|---|---|---|
| Subaerial hawaiite | Saponite + nontronite | Sap + $Sap_{35}/Chl_{65}$ + Ce |
| Submarine basalt | $Sap_{80}/Chl_{20}$ + $No_{55}/Chl_{45}$ + Chl | $Sap_{70}/Chl_{30}$ + $No_{30}/Chl_{70}$ + Ce |
| Dike hawaiite | Nontronite + Celadonite + $Cel_{70}/Chl_{30}$ | $No(2Gl)_{35}/No(1Gl)_{65}$ + $Ce_{67}/No_{33}$ + Sap |

https://doi.org/10.1346/CCMN.2008.0560612 Published online by Cambridge University Press

subaerial flow. Even if diktytaxitic voids are frequently connected to adjacent micro-vesicles, they never contain zeolites which are typically observed in the center of the vesicles or veins and veinlets.

*Clay textures in the quenched margins*

The quenched zones of the subaerial, submarine, and dike bodies exhibit a common textural organization. In all cases, the rock consists predominantly of an orange,

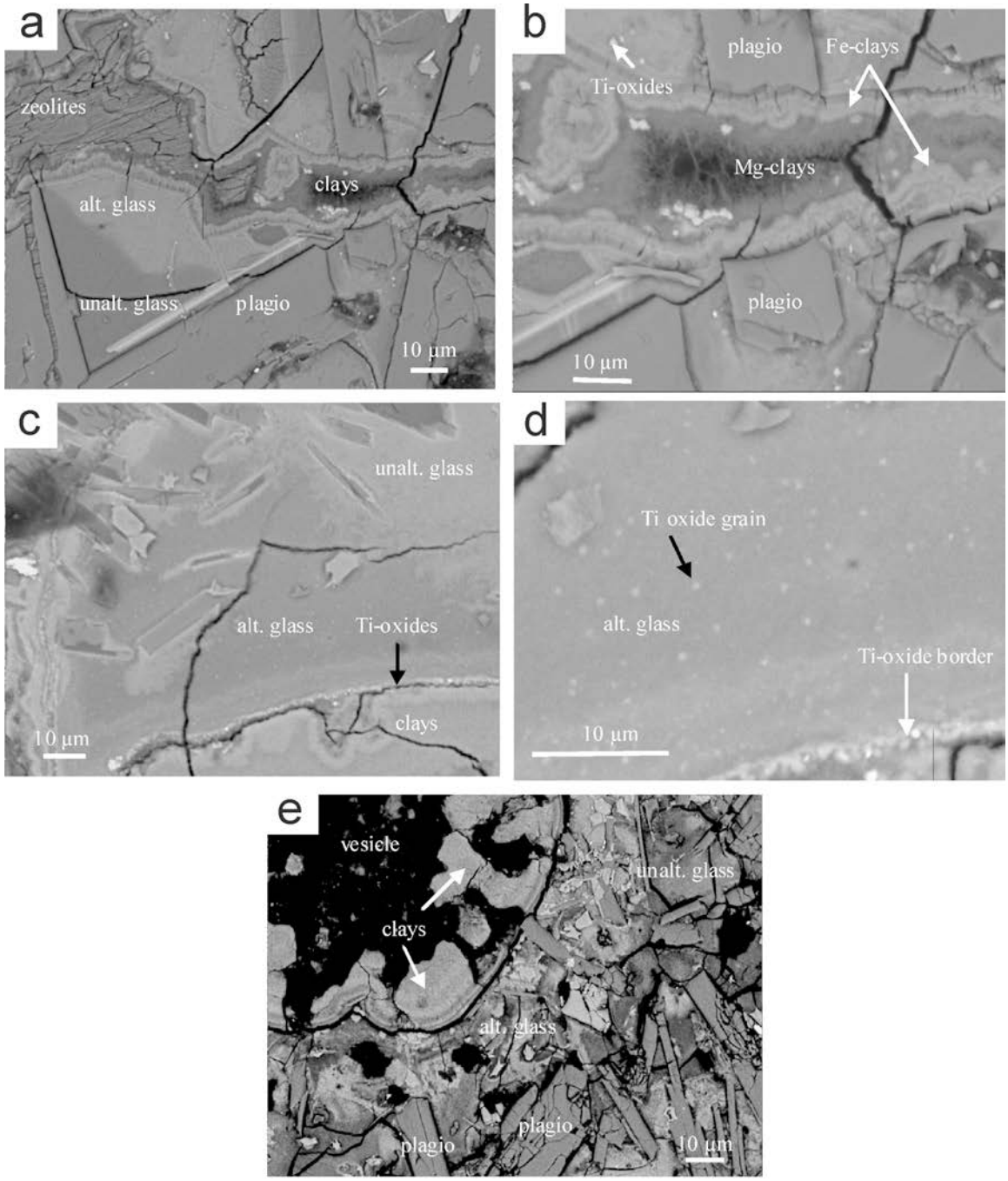


Figure 1. BSE images of thin sections from the chilled margins of the three volcanic bodies. (a,b) Subaerial flow. A vein crosscut the massive glass and plagioclase micro-phenocrysts. The altered glass is a little brighter than the fresh one. It is observed at the interface with the massive glass. The clay deposit in the vein is zoned and coats the palagonite and plagioclase interfaces. The central part of the vein is filled by zeolites. (c,d) Submarine flow. Ti oxides are scattered in the altered glass areas (bright patches). They form a continuous border at the vein interface. The clay deposits are zoned. (e) Dike. Clays form a reniform deposit in a micro-vesicle rimmed by altered glass.

https://doi.org/10.1346/CCMN.2008.0560612 Published online by Cambridge University Press

glassy matrix in which are embedded numerous plagioclase microliths and rare pyroxene microcrysts. Veins and vesicles exhibit systematically zoned clay mineral coatings on the wall-rocks (BSE observations) and zeolites in the center (Figure 1a). The veins crosscutting the quenched margins of the three volcanic bodies are related to fractures as shown by the broken plagioclase microcrystal in Figure 1b. The two fracture walls are not superimposable indicating that the percolating fluids dissolved part of the glassy matrix and the plagioclase microcrysts. The clay minerals coat all the dissolution surfaces whatever the nature of the solid phase (altered glass or plagioclase). They form concentric bright and dark rims in the outer and inner positions, respectively. The thickness of the outer rim is remarkably constant. The inner rim is formed of large crystallites oriented perpendicular to the walls and elongated toward the center of the vein (Figure 1b).

The glass in contact with veins and vesicles is systematically altered: optically, it is brown with a sharp transition to the dark, fresh glass. The contrast also appears in the BSE images: the altered zones are brighter than the fresh zones (Figure 1a,c). The boundary between unaltered and altered glass zones is roughly parallel to the walls of the veins or the vesicles. Numerous bright small grains of $TiO_2$ are disseminated in the altered glass (Figure 1c,d). They are concentrated at the clay-glass interface where they form a continuous border. Whatever the volcanic body, no evidence was found for dissolution features on the walls of vesicles or micro-vesicles. If large, they are rimmed by an altered glass zone and filled with a zoned layer of clay minerals and zeolites. A specific geodic habit of the clay deposits has been observed in the micro-vesicles of the dike quenched margins (Figure 1e).

The chemical compositions of the altered and unaltered glasses from the subaerial and submarine flows are given in Table 2. Because Ti is virtually immobile in natural alteration processes, the amount of all elements can be normalized to that of $TiO_2$ in order to study their relative variation induced by alteration (Eggleton and Keller, 1982; Staudigel and Hart, 1983; Zhou and Fyfe, 1989). The variations in the amounts of some normalized major elements are identical for the subaerial and submarine flows (Figure 2a,b): $SiO_2$, $Al_2O_3$, and FeO are depleted in the altered glass. However, MgO, MnO, $Na_2O$, and $K_2O$ are concentrated in the submarine flow while they do not change significantly or are slightly depleted in the subaerial flow. On the contrary, CaO is depleted in the submarine flow and concentrated in the subaerial flow.

Whatever the origin of the empty space in the glassy margins of the two lava flows (fractures or gas bubbles), the voids are systematically filled by a zoned clay coating: Fe-rich and Mg-rich clays in the outer and inner rims, respectively (Table 3, Figure 2c). If the vein or vesicle empty spaces are large enough, then zeolites crystallize in their center. Such zoned deposits are typical of basalt alteration (Drief and Schiffman, 2004, and references therein). This is consistent with the mineralogical composition of the clay fractions (Table 1).

### *Clay textures in the massive, crystallized inner parts*

*Subaerial flow*. Apatite and K-feldspar microcrysts are systematically present in the diktytaxitic voids which are all bordered by plagioclase phenocrysts (Figure 3a). No dissolution features are observed on the crystal faces of either the plagioclase phenocrysts or of the K-feldspar or apatite microcrysts. All the solid surfaces are coated completely by a thin layer of clay particles. Therefore, the clay minerals formed after K-feldspar, euhedral pyroxene, and apatite microcrysts. Some K-feldspar microcrysts exhibit a skeletal habit which suggests a rapid crystal growth triggered by a brutal over-saturation of the residual fluid during quenching (Lofgren, 1971a, 1971b). These crystals are widespread and randomly oriented inside the matrix (Figure 3b). Secondary electron images of small pieces of rock show that the clay particles are oriented perpendicular to the substratum of crystal faces of apatite, K-feldspars, and pyroxene microcrysts,

Table 2. Chemical composition (wt.%, microprobe analyses) of altered (Alt. G.) and unaltered (U.G.) glass from the subaerial and submarine flows.

| | Subaerial flow | | | Submarine flow | | | | | | | | | | | |
|---|---|---|---|---|---|---|---|---|---|---|---|---|---|---|---|
| | U.G. | – Alt. G. – | | U.G. | Altered glass | | | | | | | | | | |
| $SiO_2$ | 53.41 | 46.16 | 47.74 | 46.78 | 38.55 | 37.4 | 35.34 | 36.59 | 39.14 | 41.45 | 42.51 | 43.11 | 40.61 | 40.96 | 36.32 | 38.64 |
| $Al_2O_3$ | 11.56 | 12.35 | 12.26 | 11.87 | 9.67 | 8.6 | 8.71 | 8.45 | 8.68 | 8.71 | 8.91 | 10.31 | 9.34 | 8.25 | 8.99 | 7.79 |
| FeO | 16.74 | 13.44 | 12.94 | 13.52 | 19.24 | 22.02 | 22.38 | 21.33 | 20.01 | 19.27 | 19.86 | 19.64 | 21.24 | 20.63 | 20.94 | 22.4 |
| MgO | 9.27 | 4.87 | 4.64 | 4.82 | 5.11 | 6.66 | 5.71 | 6.13 | 5.43 | 6.5 | 4.82 | 4.63 | 5.11 | 4.82 | 5.65 | 4.83 |
| $TiO_2$ | 3.18 | 7.84 | 7.41 | 7.66 | 14.66 | 10.15 | 11.41 | 11.67 | 11.36 | 10.35 | 12.22 | 10.24 | 10.33 | 11.4 | 12.88 | 11.45 |
| MnO | 0 | 0.41 | 0.38 | 0.38 | 0.41 | 0.57 | 0.34 | 0.66 | 0.47 | 0.52 | 0.18 | 0.38 | 0.29 | 0.27 | 0.46 | 0.41 |
| CaO | 0.93 | 13.1 | 13.25 | 13.44 | 8.29 | 12.38 | 13.16 | 12.29 | 13.12 | 11.28 | 9.71 | 9.85 | 10.85 | 11.54 | 12.14 | 11.17 |
| $Na_2O$ | 1.09 | 1.29 | 0.99 | 1.13 | 1.58 | 0.79 | 1.39 | 1.5 | 0.84 | 0.87 | 0.84 | 0.99 | 0.84 | 1.18 | 1.22 | 1.31 |
| $K_2O$ | 3.82 | 0.54 | 0.39 | 0.41 | 2.49 | 1.43 | 1.56 | 1.38 | 0.94 | 1.05 | 0.94 | 0.84 | 1.38 | 0.95 | 1.4 | 1.99 |

All Fe is considered as $Fe^{2+}$.

https://doi.org/10.1346/CCMN.2008.0560612 Published online by Cambridge University Press

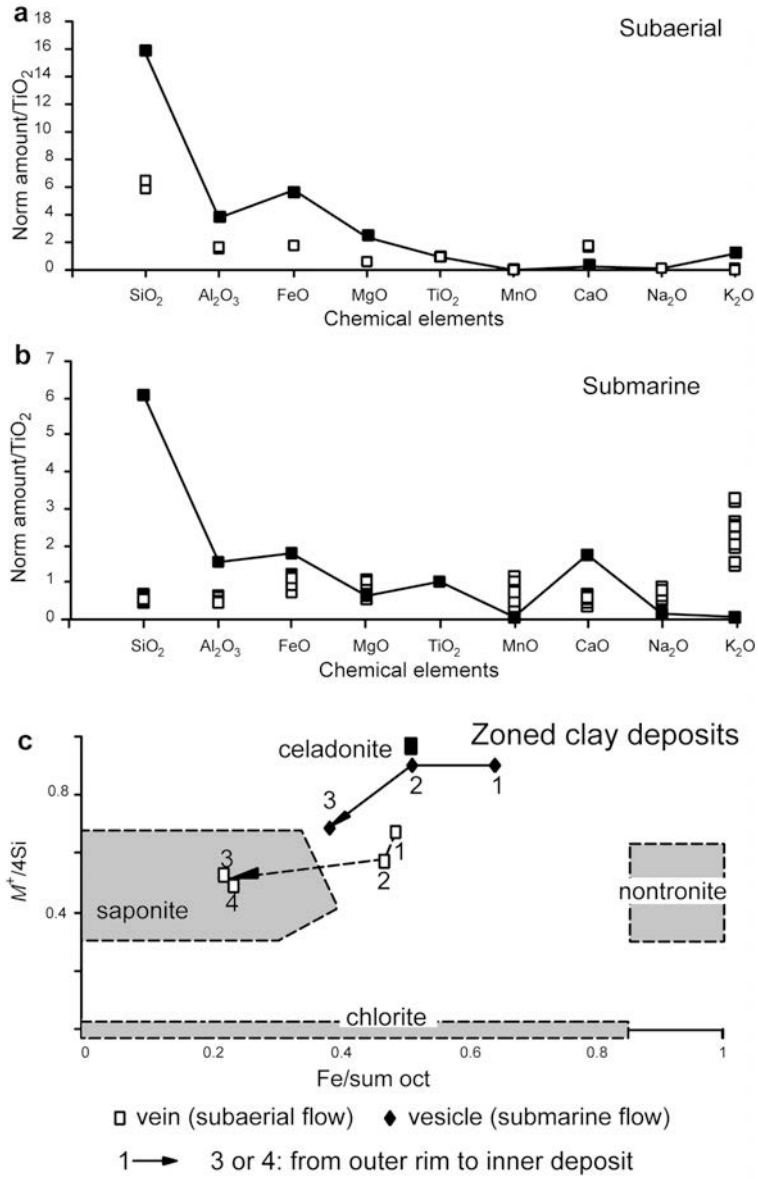


Figure 2. Amounts of major elements normalized to $TiO_2$ content (microprobe analyses) for fresh (black squares) and altered (white squares) glass for the subaerial (a) and submarine (b) flows. (c) Composition of clay minerals forming the zoned deposits in veins and vesicles from the subaerial and submarine flows plotted in the $M^+/4Si$ *vs.* Fe/sum oct cations diagram. 1 to 3−4: outer to inner rim.

*i.e.* a pallisadic texture (Figure 3c,d). None of these microcrysts was altered and no glass relics were observed.

*Submarine flow.* Micro-vesicles (diameter >100 μm) contain zoned clay mineral deposits: green clays in the outer rim and colorless in the center. Two mesostasis types were observed (BSE): a dark mesostasis (optically green) frequently connected with microvesicles of 60−100 μm in diameter (Figure 4a) and a bright mesostasis (optically black) with numerous Fe-Ti oxide grains (Figure 4b). Both consist essentially of Fe-rich clays similar to that forming the outer rim of the vesicles. This is consistent with determination of clay species (Table 1). The clay minerals are always associated with apatite and pyroxene microcrysts in the dark mesostasis and exhibit no alteration features (Figure 4c). However, the clays are randomly oriented and form an homogeneous matrix in which the microcrysts are embedded. The olivine phenocrysts are completely replaced by Fe-Mg clay minerals and a central void (Figures 4d, 5a; Table 4). The clay particles form two coating layers around the dissolution void (BSE): the outer layer is massive; the inner one consists of large particles oriented toward the center. Large clay particles

https://doi.org/10.1346/CCMN.2008.0560612 Published online by Cambridge University Press

Table 3. Chemical composition (wt.%, microprobe analyses) of clay minerals forming the zoned deposits of veins and vesicles in the glassy chilled margins of the subaerial and submarine flows. All Fe is considered as $Fe^{3+}$.

| | Subaerial flow (vein) | | | | Submarine flow (vesicle) | | |
|---|---|---|---|---|---|---|---|
| | 1 | 2 | 3 | 4 | 1 | 2 | 3 |
| Si | 3.56 | 3.51 | 3.27 | 3.35 | 3.28 | 3.38 | 3.26 |
| $^{IV}Al$ | 0.44 | 0.49 | 0.73 | 0.65 | 0.72 | 0.62 | 0.74 |
| $^{VI}Al$ | 0.44 | 0.48 | 0.17 | 0.19 | 0.27 | 0.45 | 0.24 |
| $Fe^{3+}$ | 1.04 | 1.06 | 0.61 | 0.64 | 1.36 | 1.1 | 0.96 |
| Mg | 0.68 | 0.61 | 1.96 | 1.88 | 0.43 | 0.54 | 1.26 |
| Ti | 0.03 | 0.03 | 0.01 | 0 | 0.05 | 0.05 | 0.02 |
| Mn | 0.01 | 0 | 0 | 0.1 | 0.01 | 0 | 0.01 |
| Sum oct | 2.2 | 2.17 | 2.75 | 2.7 | 2.11 | 2.13 | 2.48 |
| Ca | 0.04 | 0.06 | 0.1 | 0.1 | 0.1 | 0.12 | 0.14 |
| Na | 0.07 | 0.09 | 0.09 | 0.08 | 0.05 | 0.09 | 0.08 |
| K | 0.36 | 0.38 | 0.14 | 0.13 | 0.49 | 0.43 | 0.2 |

undoubtedly formed through a geometrical selection process typical of crystal growth in porous media (Grigor'ev, 1965; Billault *et al*., 2003). This indicates that olivine phenocrysts were altered by an aqueous solution. No glass remains were observed in the dark or bright mesostases. The skeletal habit of the Fe-Ti oxides

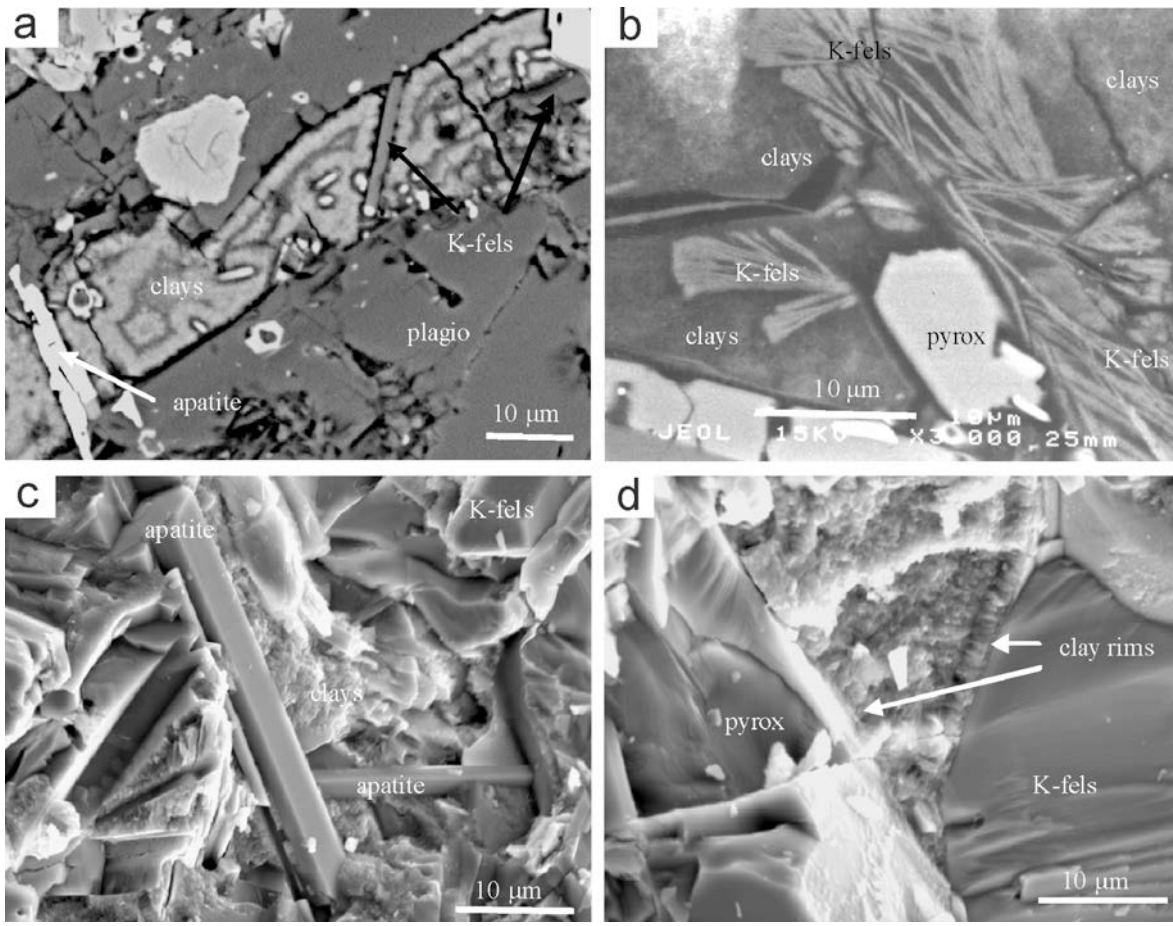


Figure 3. Subaerial flow. SEM images of diktytaxitic voids. (a) BSE image showing the clay deposit zoning and the presence of K-feldspar and apatite micro-crystals. (b) Detail of the BSE image showing skeletal K-feldspar crystals embedded in a clay matrix. (c) SE image of a diktytaxitic void showing the presence of K-feldspar and a euhedral apatite crystal embedded in the clay matrix. (d) SE image of the pallisadic texture of clay particles forming a regular rim on K-feldspar and pyroxene crystals.

https://doi.org/10.1346/CCMN.2008.0560612 Published online by Cambridge University Press

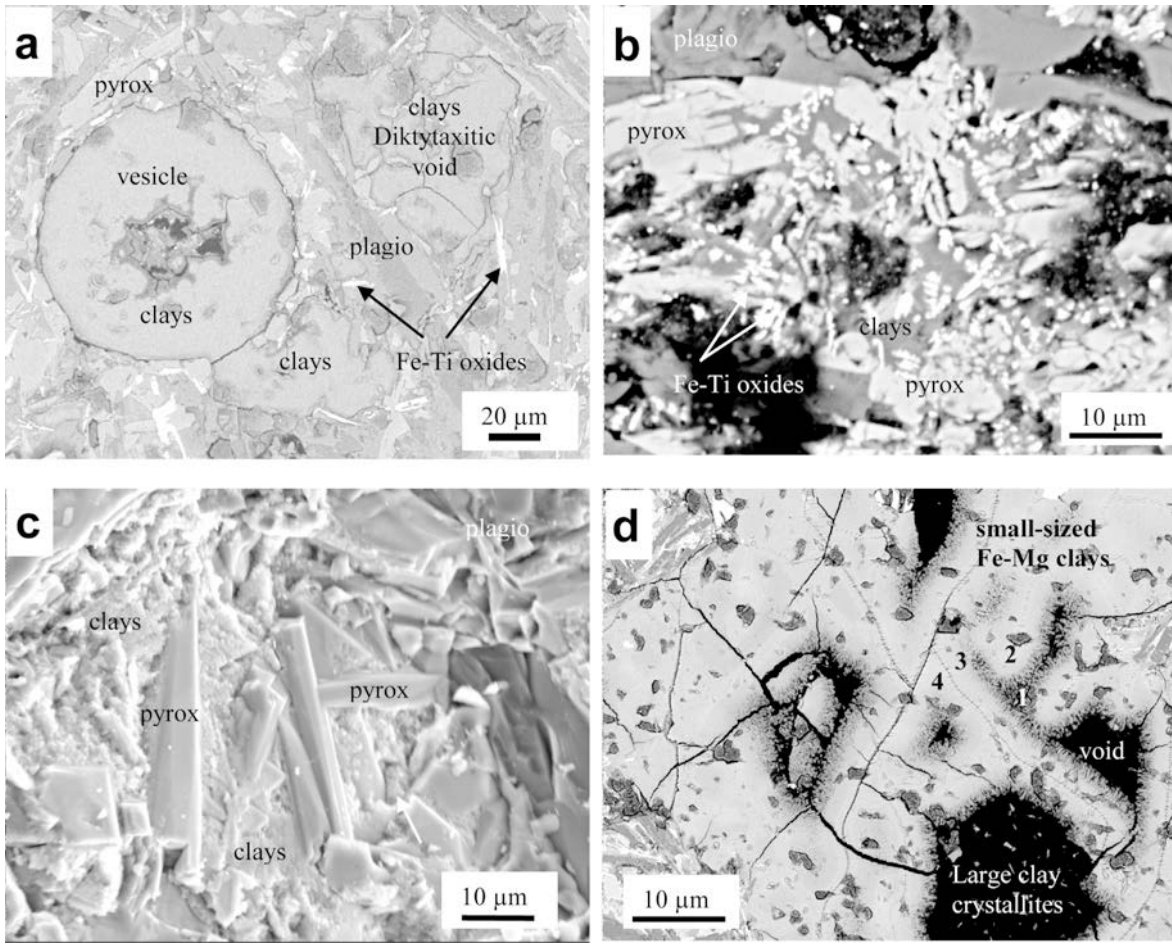


Figure 4. Submarine flow. SEM images of diktytaxitic voids and an olivine phenocryst. (a) BSE image showing the connection between a vesicle and the diktytaxitic voids. (b) BSE image of a black mesostasis formed of numerous Fe-Ti oxides scattered in a clay matrix. (c) SEM image of a diktytaxitic void showing the presence of euhedral pyroxene microcrysts embedded in a randomly oriented clay matrix. (d) BSE image of an olivine phenocryst pseudomorphosed by clay minerals. Numbers indicate the zones analyzed (Table 4).

Table 4. Chemical composition (wt.%, microprobe analyses) of clay minerals forming the zoned deposits in a completely pseudomorphosed olivine phenocryst of the submarine flow. All Fe is considered as $Fe^{3+}$.

| | Olivine pseudomorph | | | |
|---|---|---|---|---|
| | 1 | 2 | 3 | 4 |
| Si | 3.19 | 3.23 | 3.57 | 3.55 |
| $^{IV}Al$ | 0.81 | 0.77 | 0.43 | 0.45 |
| $^{VI}Al$ | 0.1 | 0.22 | 0.49 | 0.57 |
| $Fe^{3+}$ | 1.23 | 1.08 | 0.94 | 0.87 |
| Mg | 1.1 | 1.15 | 0.68 | 0.67 |
| Ti | 0.01 | 0 | 0.01 | 0.02 |
| Mn | 0.02 | 0.02 | 0.01 | 0.01 |
| Sum oct | 2.45 | 2.47 | 2.13 | 2.14 |
| Ca | 0.1 | 0.08 | 0.08 | 0.07 |
| Na | 0.04 | 0.05 | 0.03 | 0.06 |
| K | 0.35 | 0.31 | 0.53 | 0.49 |

suggests that they formed during a rapid quenching event. Their particular crystal habit is typically observed within a glassy matrix (Kontak *et al.*, 2002). As the olivine phenocrysts have undoubtedly been altered, alteration of the glassy matrix of the black mesostasis is also suspected. However, this remains speculative because the chemical compositions of the glassy matrix and the Fe-rich clay minerals are very different.

*Dike.* Because most of the plagioclase, K-feldspar, or pyroxene pheno- or microcrysts are perfectly euhedral, the diktytaxitic voids have angular borders (Figure 6a,b). The clay coatings form two concentric layers, the thickness of which depends on the void size (BSE). Clay coatings systematically cover apatite and Fe-Ti oxide microcrysts. Remarkably, whatever their size, the voids are never filled completely. A residual open space in the center persists. The central free space of the largest voids is more irregularly shaped and looks like micro-geoda (SE): the inner clay-coating exhibits a

https://doi.org/10.1346/CCMN.2008.0560612 Published online by Cambridge University Press

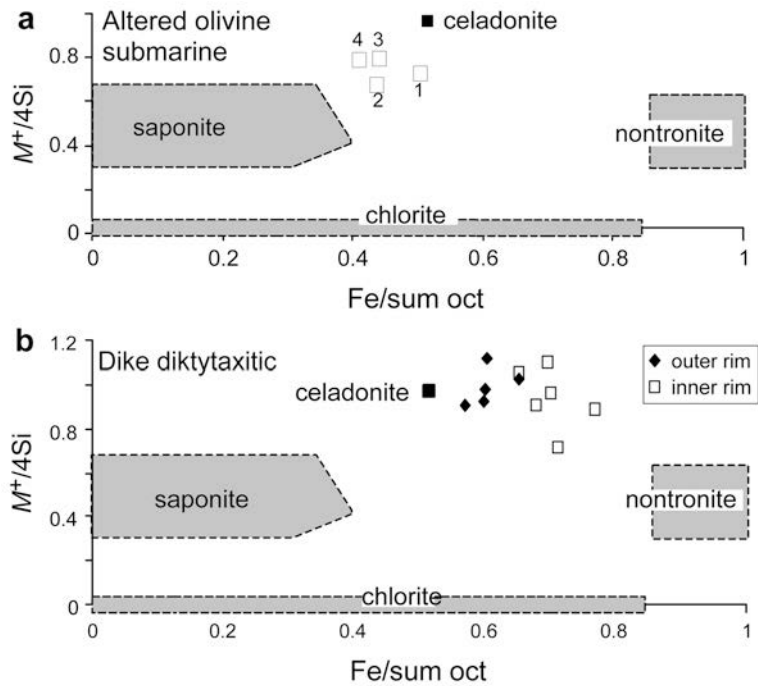


Figure 5. Composition of clay minerals zoning in (a) a pseudomorphosed olivine phenocryst (submarine flow) and (b) a diktytaxitic void (dike) plotted in the $M^+$/4Si *vs.* Fe/sum oct diagram.

reniform habit (Figure 6c,d). Using greater magnification, the texture of the reniform inner clay-coating appears very unusual: it is organized by the random stacking of apatite needles, each being covered by a clay 'muff' (Figure 6e,f). The thickness of the clay coating on each individual needle is perfectly constant. Large, free spaces separate the needles making the clay-apatite deposit porous.

The inner clay coating is always more Fe-rich than the outer one (Table 5; Figure 5b). The composition of the clays plots between the celadonite and nontronite end-members (Mas *et al.*, 2008). This is consistent with the mineralogical composition (Table 1) which is dominated by high-charge nontronite and $Ce_{67}/No_{33}$ mixed-layer minerals. This clay mineral assemblage forms the muff covering each apatite needle and the inner rim of the diktytaxitic voids. The outer rim is composed of Fe-rich clays associated with saponite.

### *Chemical composition of bulk rocks and clay fraction*

*Major and trace chemical elements*. The chemical compositions of the basalt-hawaiite rocks from Mururoa Atoll are given for major, trace, and *REE* of the bulk rocks (Table 6) and for their <2 μm fraction (Table 7).

Table 5. Chemical composition (wt.%, microprobe analyses) of clay minerals forming the zoned deposits coating the angular diktytaxitic voids of the dike. All Fe is considered as $Fe^{3+}$.

| | Outer rim | | | | | Inner rim | | | | | |
|---|---|---|---|---|---|---|---|---|---|---|---|
| | 1 | 2 | 3 | 4 | 5 | 1 | 2 | 3 | 4 | 5 | 6 |
| Si | 3.40 | 3.36 | 3.52 | 3.47 | 3.43 | 3.30 | 3.25 | 3.27 | 3.30 | 3.23 | 3.27 |
| $^{IV}$Al | 0.60 | 0.64 | 0.48 | 0.53 | 0.57 | 0.70 | 0.75 | 0.73 | 0.70 | 0.77 | 0.73 |
| $^{VI}$Al | 0.41 | 0.48 | 0.52 | 0.45 | 0.43 | 0.16 | 0.11 | 0.11 | 0.02 | 0.01 | 0.19 |
| $Fe^{3+}$ | 1.30 | 1.20 | 1.14 | 1.20 | 1.22 | 1.45 | 1.47 | 1.50 | 1.57 | 1.65 | 1.38 |
| Mg | 0.24 | 0.27 | 0.32 | 0.33 | 0.36 | 0.49 | 0.50 | 0.48 | 0.55 | 0.43 | 0.50 |
| Ti | 0.02 | 0.03 | 0.01 | 0.01 | 0.03 | 0.02 | 0.03 | 0.03 | 0.05 | 0.05 | 0.02 |
| Mn | 0.01 | 0.01 | 0.00 | 0.00 | 0.01 | 0.01 | 0.01 | 0.01 | 0.01 | 0.01 | 0.00 |
| Sum oct | 1.99 | 1.99 | 2.00 | 2.00 | 2.04 | 2.14 | 2.11 | 2.14 | 2.21 | 2.15 | 2.12 |
| Ca | 0.11 | 0.09 | 0.10 | 0.09 | 0.08 | 0.08 | 0.12 | 0.09 | 0.08 | 0.06 | 0.14 |
| Na | 0.06 | 0.11 | 0.11 | 0.13 | 0.40 | 0.03 | 0.08 | 0.06 | 0.05 | 0.06 | 0.08 |
| K | 0.59 | 0.85 | 0.48 | 0.54 | 0.59 | 0.55 | 0.57 | 0.56 | 0.37 | 0.48 | 0.49 |
| $M^+$ | 0.87 | 0.94 | 0.80 | 0.85 | 0.79 | 0.75 | 0.89 | 0.79 | 0.59 | 0.72 | 0.86 |

https://doi.org/10.1346/CCMN.2008.0560612 Published online by Cambridge University Press

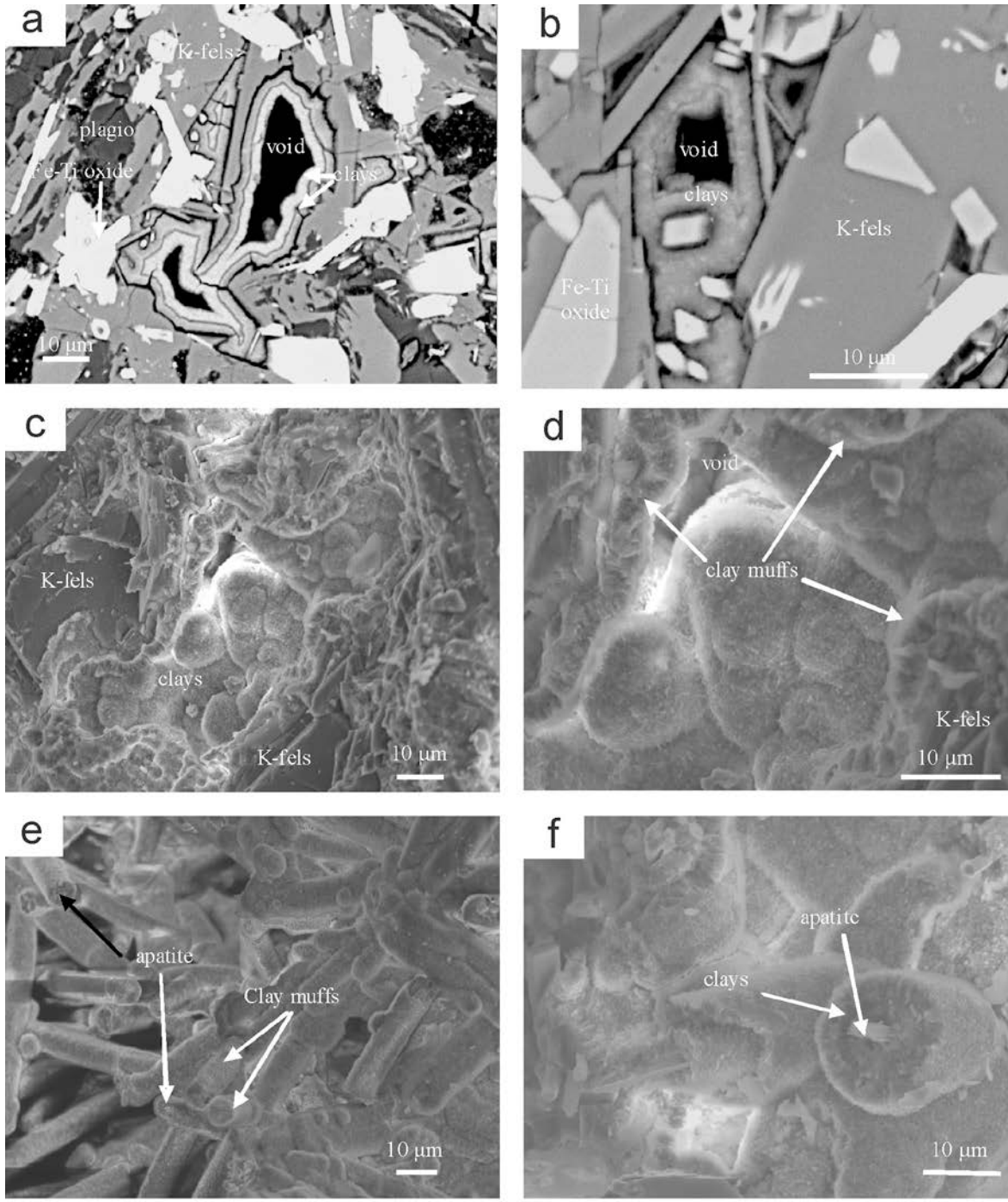


Figure 6. Dike. SEM images of diktytaxitic voids. (a) BSE image of a regular double rim coating the walls of two angularly shaped diktytaxitic voids in which the central parts remain empty. (b) BSE image of the inner clay rim exhibits a reniform habit in the central void. (c) SEM image of a reniform deposit in a micro-geoda. (d) detail of the reniform deposit. (e) Clays form 'muffs' covering all the apatite microcrysts. (f) Detail of the picture showing the perfectly ordered clay particle organization in the apatite 'muffs'.

$K_2O$, $H_2O$, and $P_2O_5$ are concentrated in the mesostasis. They contribute to the formation of K-feldspar, celadonite-nontronite and apatite. Because the mesostasis is a fine-grained material, its trace elements and *REE* composition may be approached by chemical analysis of the <2 µm fraction. These compositions are presented as spider diagrams of the clay fractions. The amounts are normalized to the bulk-rock composition of the massive

https://doi.org/10.1346/CCMN.2008.0560612 Published online by Cambridge University Press

Table 6. Bulk-rock chemical composition (major elements).

| | Subaerial | | | Submarine | | | Dike | |
|---|---|---|---|---|---|---|---|---|
| | Chilled margin | Massive inner part | Brecciated | Chilled margin | Massive inner part | Brecciated | Chilled margin | Massive inner part |
| Depth (m) | −644.1 | −642.4 | −640.7 | −697.6 | −697.00 | −695.9 | −718.45 | −719.45 |
| $SiO_2$ | 42.43 | 46.64 | 48.19 | 37.87 | 43.32 | 41.80 | 46.53 | 44.31 |
| $Al_2O_3$ | 14.31 | 15.66 | 16.21 | 13.24 | 14.9 | 14.74 | 15.36 | 14.95 |
| $Fe_2O_3$ | 11.72 | 12.61 | 10.79 | 14.73 | 13.39 | 12.12 | 10.03 | 13.11 |
| $TiO_2$ | 4.80 | 3.56 | 3.28 | 5.50 | 4.56 | 4.46 | 3.32 | 3.88 |
| MgO | 6.19 | 4.40 | 3.80 | 6.51 | 4.83 | 5.77 | 2.05 | 3.71 |
| MnO | 0.09 | 0.19 | 0.15 | 0.19 | 0.21 | 0.12 | 0.19 | 0.12 |
| CaO | 5.10 | 8.53 | 8.58 | 5.38 | 10.31 | 4.43 | 6.11 | 7.48 |
| $Na_2O$ | 2.64 | 3.64 | 3.63 | 2.81 | 2.30 | 4.14 | 5.14 | 3.48 |
| $K_2O$ | 1.70 | 2.26 | 2.54 | 1.66 | 1.73 | 2.01 | 3.26 | 2.59 |
| $P_2O_5$ | 0.76 | 1.04 | 0.96 | 0.75 | 0.55 | 0.31 | 0.85 | 0.69 |
| LOI | 10.23 | 1.87 | 2.30 | 11.84 | 3.90 | 10.02 | 7.15 | 5.69 |
| Total | 99.97 | 100.4 | 100.43 | 100.48 | 100.00 | 99.92 | 99.99 | 100.01 |

LOI: loss on ignition
All Fe is considered as $Fe^{2+}$.

Table 7. Amounts of trace elements and *REE* in the massive rocks and in the <2 μm fractions from the chilled margins and massive parts of the three volcanic bodies.

| | Subaerial | | | | Submarine | | | | Dike | | |
|---|---|---|---|---|---|---|---|---|---|---|---|
| | Chilled margin | Massive body | | Brecciated | Chilled margin | Massive body | | Brecciated | Massive body | | Chilled margin |
| | Clays | Clays | Rock | Clays | Clays | Clays | Rock | Clays | Clays | Rock | Clays |
| As | 0.61 | 2.41 | 1.15 | 0.94 | 0.96 | 0.92 | 0.41 | 1.01 | 1.49 | 0.31 | 0.66 |
| Ba | 95.2 | 323.00 | 485.83 | 261.00 | 141.00 | 132.00 | 252.55 | 97.1 | 228.00 | 258.5 | 342.00 |
| Be | 4.72 | 6.77 | 1.86 | 4.66 | 3.07 | 3.27 | 1.42 | 2.57 | 5.47 | 0.94 | 3.05 |
| Bi | 0.1 | 0.29 | 0.00 | 0.00 | 0.00 | 0.00 | 0.00 | 0.06 | 0.00 | 0.00 | 0.00 |
| Cd | 0.92 | 1.47 | 0.35 | 1.02 | 0.36 | 0.47 | 0.28 | 0.44 | 0.75 | 0.25 | 0.61 |
| Co | 65.4 | 266.00 | 25.44 | 158.00 | 79.2 | 129.00 | 57.33 | 80.8 | 146.00 | 26.41 | 201.00 |
| Cr | 9.3 | 109.00 | 3.19 | 55.6 | 99.9 | 75.1 | 373.53 | 61.3 | 25.1 | 0.00 | 34.00 |
| Cs | 0.69 | 0.78 | 0.31 | 1.27 | 0.96 | 1.12 | 0.75 | 1.35 | 1.34 | 0.29 | 1.94 |
| Cu | 157.00 | 44.00 | 15.44 | 32.7 | 152.00 | 149.00 | 53.47 | 180.00 | 12.7 | 7.55 | 17.3 |
| Ga | 26.9 | 29.8 | 29.21 | 23.5 | 29.2 | 29.9 | 29.98 | 31.2 | 37.9 | 20.82 | 39.2 |
| Ge | 2.37 | 1.24 | 1.14 | 1.35 | 2.44 | 1.71 | 1.56 | 2.19 | 1.41 | 0.77 | 3.51 |
| Hf | 14.00 | 13.6 | 10.09 | 11.2 | 7.09 | 6.76 | 6.79 | 7.09 | 20.6 | 6.69 | 8.55 |
| In | 0.17 | 0.00 | 0.06 | 0.00 | 0.00 | 0.00 | 0.1 | 0.00 | 0.00 | 0.07 | 0.00 |
| Mo | 2.89 | 23.00 | 2.15 | 9.96 | 4.28 | 0.99 | 1.19 | 6.37 | 7.42 | 0.65 | 7.26 |
| Nb | 111.00 | 103.00 | 80.6 | 87.7 | 57.4 | 59.5 | 48.64 | 56.5 | 109.00 | 49.4 | 69.5 |
| Ni | 109.00 | 37.00 | 3.84 | 52.5 | 129.00 | 217.00 | 89.9 | 121.00 | 16.6 | 3.79 | 259.00 |
| Pb total | 5.24 | 9.79 | 4.09 | 6.65 | 2.91 | 4.16 | 2.5 | 5.16 | 8.53 | 4.15 | 5.89 |
| Rb | 35.1 | 47.00 | 38.59 | 50.3 | 52.2 | 59.1 | 38.66 | 56.00 | 96.2 | 34.47 | 101.00 |
| Sb | 0.16 | 0.32 | 0.08 | 0.15 | 0.2 | 0.13 | 0.09 | 0.17 | 0.23 | 0.07 | 0.12 |
| Sn | 7.37 | 12.6 | 2.71 | 6.44 | 4.37 | 6.61 | 2.75 | 19.00 | 8.59 | 1.88 | 6.42 |
| Sr | 119.00 | 559.00 | 857.14 | 400.00 | 169.00 | 307.00 | 683.92 | 175.00 | 976.00 | 931.07 | 538.00 |
| Ta | 6.9 | 7.27 | 6.09 | 6.47 | 4.16 | 4.08 | 3.55 | 3.95 | 9.41 | 3.87 | 5.46 |
| Th | 10.8 | 16.3 | 7.03 | 10.5 | 4.2 | 8.19 | 3.28 | 5.35 | 12.4 | 3.56 | 6.36 |
| U | 4.83 | 7.1 | 2.12 | 3.8 | 2.2 | 4.8 | 1.95 | 1.93 | 4.34 | 1.39 | 3.32 |
| V | 264.00 | 53.3 | 218.94 | 144.00 | 297.00 | 85.7 | 364.72 | 215.00 | 47.00 | 157.62 | 116.00 |
| W | 2.41 | 19.1 | 0.27 | 10.6 | 2.21 | 3.89 | 0.21 | 2.6 | 6.02 | 0.3 | 6.31 |
| Y | 36.6 | 58.00 | 36.67 | 41.8 | 31.2 | 35.00 | 27.12 | 27.7 | 30.8 | 20.38 | 27.8 |
| Zn | 220.00 | 242.00 | 169.22 | 188.00 | 221.00 | 202.00 | 170.45 | 376.00 | 172.00 | 124.29 | 242.00 |
| Zr | 725.00 | 742.00 | 436.22 | 573.00 | 329.00 | 388.00 | 299.77 | 316.00 | 1043.00 | 277.79 | 406.00 |

https://doi.org/10.1346/CCMN.2008.0560612 Published online by Cambridge University Press

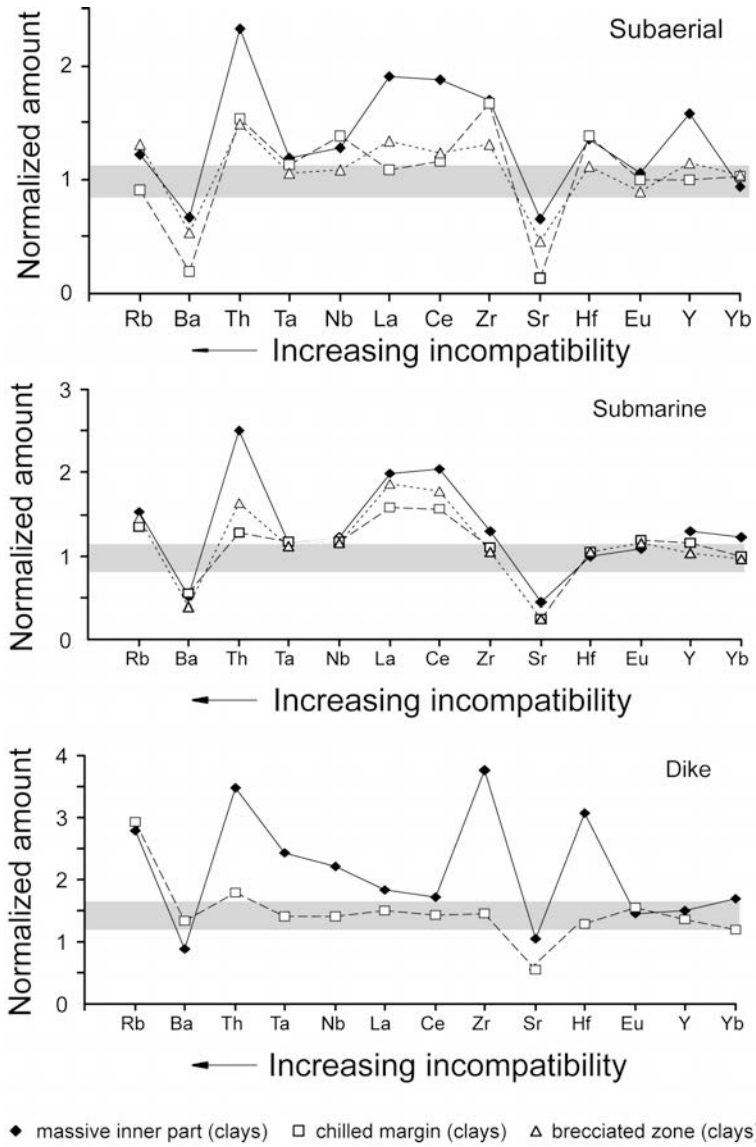


Figure 7. Amounts of incompatible elements in the <2 μm fraction normalized to the bulk-rock composition for the three volcanic bodies (spider diagrams). Gray zone: experimental error domain for the bulk-rock composition.

crystallized inner part (Figure 7). The spider diagrams exhibit two common properties: (1) The clay fractions of the massive rock are richer in the most incompatible elements (from Rb to Sr) than that of the glassy chilled margins. The less incompatible elements (from Hf to Yb) are slightly or not enriched in the clay fractions. (2) Negative anomalies for Ba and Sr: the negative Ba anomaly is related to the difficulty for clays to accept such large bivalent cations in their interlayer region. Under natural conditions, the cation exchange favors Rb ions which are monovalent. The other negative anomaly concerns Sr which is depleted in the clay minerals. Two different processes can be envisaged: fractionation by feldspars (end of the magma crystallization period) or leaching during alteration (post-magmatic interaction with fluids). Leaching promotes a positive correlation between Sr and Ca depletion.

The spider diagrams of the clay fractions in the dike are significantly different from those of the subaerial and submarine flows. They are more enriched in Ta, Nb, Zr, and Hf. This could indicate that fractionation in the two lava flows and the dike occurred under different conditions (mono- or bi-phased residual liquid).

The chemical differences between the massive rock and its clay fraction are enhanced in Figure 8 where the relative amounts of *REE* are normalized to the primitive mantle composition (Sun and McDonough, 1989). Considering the massive inner parts, the amounts of light rare-earth elements (*LREE)* from La to Eu are systematically larger in the clay fraction than in the bulk

https://doi.org/10.1346/CCMN.2008.0560612 Published online by Cambridge University Press

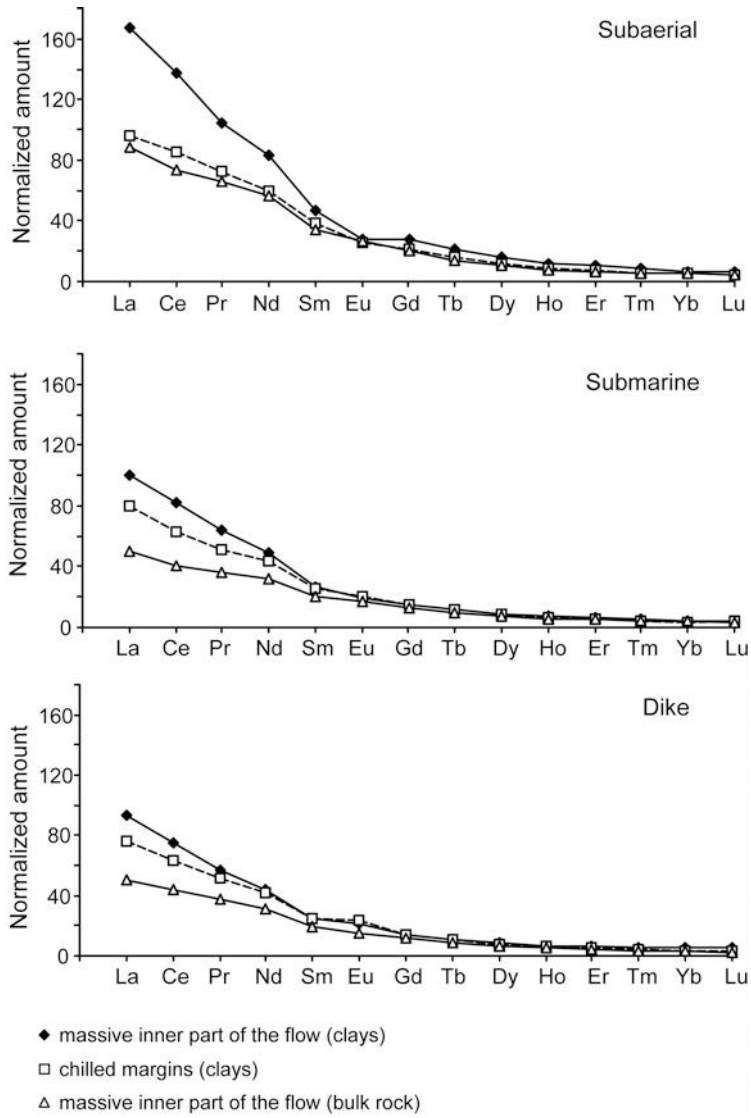


Figure 8. Amounts of *REE* normalized to the primitive mantle composition (Sun and McDonough, 1989) of the clay fractions of the chilled and massive inner parts and the bulk rocks of the three volcanic bodies.

rock, whatever the volcanic body, while that of the heavy rare-earth elements (*HREE*) from Gd to Lu are remarkably similar. The relative enrichment in *LREE* in the clay fraction is significantly less in the chilled margins.

*Oxygen isotopic composition.* The clay fraction of the three volcanic bodies presents larger $\delta^{18}O$ values in the chilled or brecciated margins than in the corresponding massive facies (Table 8). The difference could be related either to a varying degree of alteration in a single fluid-rock system or to the presence of two isolated fluid-rock systems located in the chilled margins (alteration process) and the massive inner parts at the moment of clay mineral crystallization (post-magmatic processes).

*The $^{87}Sr/^{86}Sr$ and $^{87}Rb/^{86}Sr$ ratios.* The ratios are given in Table 8. Because the three volcanic bodies have nearly the same age: 11.5 Ma ± 0.3 (Caroff, 1992), the initial $^{87}Sr/^{86}Sr$ ratio can be calculated for the bulk rocks using 0.70915 and 7.6 ppm for average $^{87}Sr/^{86}Sr$ value and Sr amounts in sea water, respectively (DePaolo, 1986; Veizer, 1989). The variations observed between measured and calculated values (Table 9) have been attributed to interactions of the rocks with sea water (Maury *et al.*, 1992; Guille *et al.*, 1993). Table 8 shows that the quenched margins of the subaerial and submarine flows have larger $^{87}Sr/^{86}Sr$ ratio values than the corresponding massive parts. The reverse is observed in the dike. The $^{87}Sr/^{86}Sr$ *vs.* $^{87}Rb/^{86}Sr$ variation shows that the composition of the bulk rocks and the clay

https://doi.org/10.1346/CCMN.2008.0560612 Published online by Cambridge University Press

Table 8. Stable ($^{18}O/^{16}O$) and radioactive ($^{87}Sr/^{86}Sr$ and $^{87}Rb/^{86}Sr$) isotope ratios of the bulk rock and the clay fractions from the chilled margins and the massive crystallized inner parts of the subaerial and submarine flows, and of the dike.

| | Subaerial | | | | Submarine | | | | Dike | | | |
|---|---|---|---|---|---|---|---|---|---|---|---|---|
| | Chilled margin | | Massive body | | Brecciated | | Chilled margin | | Massive body | | Brecciated | |
| | Clays | Rock | Clays | Rock | Clays | Rock | Clays | Rock | Clays | Rock | Clays | Rock |
| $^{87}Sr/^{86}Sr$ | 0.704432 | 0.703704 | 0.704039 | 0.703684 | 0.703788 | 0.703761 | 0.7 04547 | 0.703814 | 0.704139 | 0.703453 | 0.705076 | 0.704516 |
| $^{87}Rb/^{86}Sr$ | 0.89 | 0.066 | 0.24 | 0.148 | 0.368 | 0.071 | 0.916 | 0.242 | 0.548 | 0.117 | 0.966 | 0.166 |
| $^{18}O/^{16}O$ | 18.8 | n.d. | 12.5 | n.d. | 14.7 | n.d. | 18.6 | n.d. | 16.9 | n.d. | 18.3 | n.d. |

| | Dike | | | |
|---|---|---|---|---|
| | Chilled margin | | Massive body | |
| | Clays | Rock | Clays | Rock |
| $^{87}Sr/^{86}Sr$ | 0.704048 | 0.703672 | 0.704137 | 0.703887 |
| $^{87}Rb/^{86}Sr$ | 0.592 | 0.033 | 0.296 | 0.075 |
| $^{18}O/^{16}O$ | 17.9 | n.d. | 16.0 | n.d. |

Table 9. Measured and calculated $^{87}Sr/^{86}Sr$ ratio values in the massive inner parts of the subaerial and submarine flows and of the dike. The ratios were calculated assuming a 11.5 Ma age using 0.70915 and 7.6 ppm for the average $^{87}Sr/^{86}Sr$ value and amounts of Sr in sea water, respectively

| Volcanic body | $^{87}Sr/^{86}Sr$ measured | $^{87}Sr/^{86}Sr$ calculated |
|---|---|---|
| Subaerial | 0.703684 | 0.703673 |
| Submarine | 0.703453 | 0.703433 |
| Dike | 0.703887 | 0.703874 |

fractions are scattered around the 11.5 Ma isochron (Figure 9), the greatest $^{87}Rb/^{86}Sr$ ratio values being found in the clays from the quenched margins. This indicates that the Rb-Sr chemical system cannot be considered as perfectly closed in the three volcanic bodies.

## DISCUSSION

### *Basaltic glass alteration in vesicles and veins of the quenched margins*

Veins and vesicles are systematically sealed by zoned clay coatings: Fe-rich clays, Mg-rich clays, and zeolites from the outer through intermediate to inner deposits, respectively. The basalt-hawaiite glass in the chilled margins is altered in the vicinity of veins and vesicles. Compared to the unaltered glass, it is systematically depleted with respect to $SiO_2$, $Al_2O_3$, and FeO. It is also CaO depleted in the submarine flow. Conversely, the altered glass is relatively enriched in MgO, MnO, $Na_2O$, and $K_2O$. Thorseth *et al.* (1991) showed that $TiO_2$ may be locally soluble in some specific zones (white palagonite) where acidic conditions prevail (pH <3). However, it becomes insoluble in the brown palagonite (pH >3). This explains the presence of many small Ti oxide grains scattered in the altered glass of the

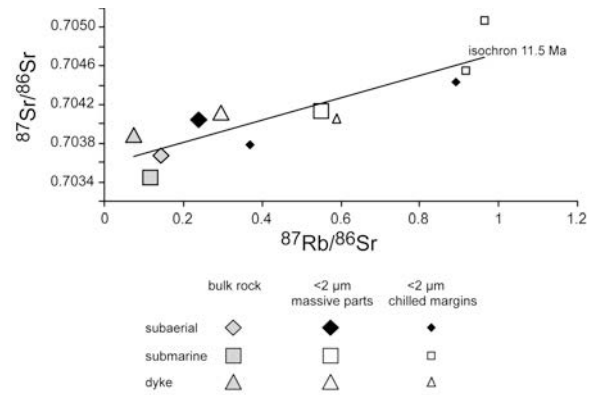


Figure 9. Relationship between the $^{87}Sr/^{86}Sr$ and $^{87}Rb/^{86}Sr$ ratios for the bulk rocks and the <2 µm fraction extracted from the massive parts and the chilled margins of the three volcanic bodies. The line represents the 11.5 Ma isochron.

https://doi.org/10.1346/CCMN.2008.0560612 Published online by Cambridge University Press

subaerial and submarine flows or accumulated along the interface of the altered glass at the base of the Fe-rich clay coatings.

How can alteration of the basalt-hawaiite glass form the clay mineral zoning observed in both veins and vesicles? Since Bonorino's pioneer work (1959), zoned mineral fillings in veins have been studied from mineralogical, chemical, and thermodynamic points of view. The inward propagation of alteration processes (mainly the dissolution of the pre-existing solids) is controlled by chemical gradients between fractures and rocks. The gradients themselves are controlled either by the growth of secondary mineral phases in the free spaces or by the rate of renewal of the dissolving solution in closed or open systems, respectively (Meunier, 1994). Some of the chemical components of the altered glass are depleted because they are solubilized (Si, Ca) or consumed by the first secondary minerals to be formed (Al, Fe): nontronite-type clays. Titanium precipitates as Ti oxide micro-aggregates (brookite?) inside the altered glass. As nontronite crystals grow, the dissolution front progresses inward into the altered glass, *i.e.* retreating interface (Banfield and Barker, 1998). The retreating interface makes the Ti oxide grains accumulate along the interface between altered glass and clays. Concomitantly, the glass dissolution increases the amounts of silica and Mg in solution. This triggers the precipitation of more magnesian phyllosilicates (Fe-saponite, chlorite, C/S MLMs), the nucleation and growth of which are favored by epitaxial effects on the free outer surfaces of the nontronite-type crystals. The increasing amount of Mg incorporated in the newly formed clay phases depletes the solution with Mg. Consequently, the last phases to precipitate are Mg-free, *i.e.* zeolites. The different steps of formation of the zoned deposit in a vein can be represented schematically (Figure 10). From the fracture-opening (time $t_0$) to the final sealing by zeolite deposition (time $t_x$), the Fe- and Mg-rich clay minerals nucleate and grow in opposite directions while the fluid-altered glass interface retreats. A similar process works in the vesicles but, here, the altered glass–clay interface is not outlined by Ti oxide grains, indicating that the interface is not retreating. Thus, the crystallization of the clays and zeolites is probably supported by the diffusion of the dissolved components from the surrounding altered glass.

### *Mesostasis of the inner massive parts: the glass precursor problem*

*Subaerial and submarine flows.* During the cooling stage, the composition of a magma changes with increasing crystallization ratio ($C_r$), *i.e.* crystalline material mass *vs.* magma mass ratio. Consequently, the composition of the ultimate liquid giving the intergranular glass varies from andesitic to rhyolitic types

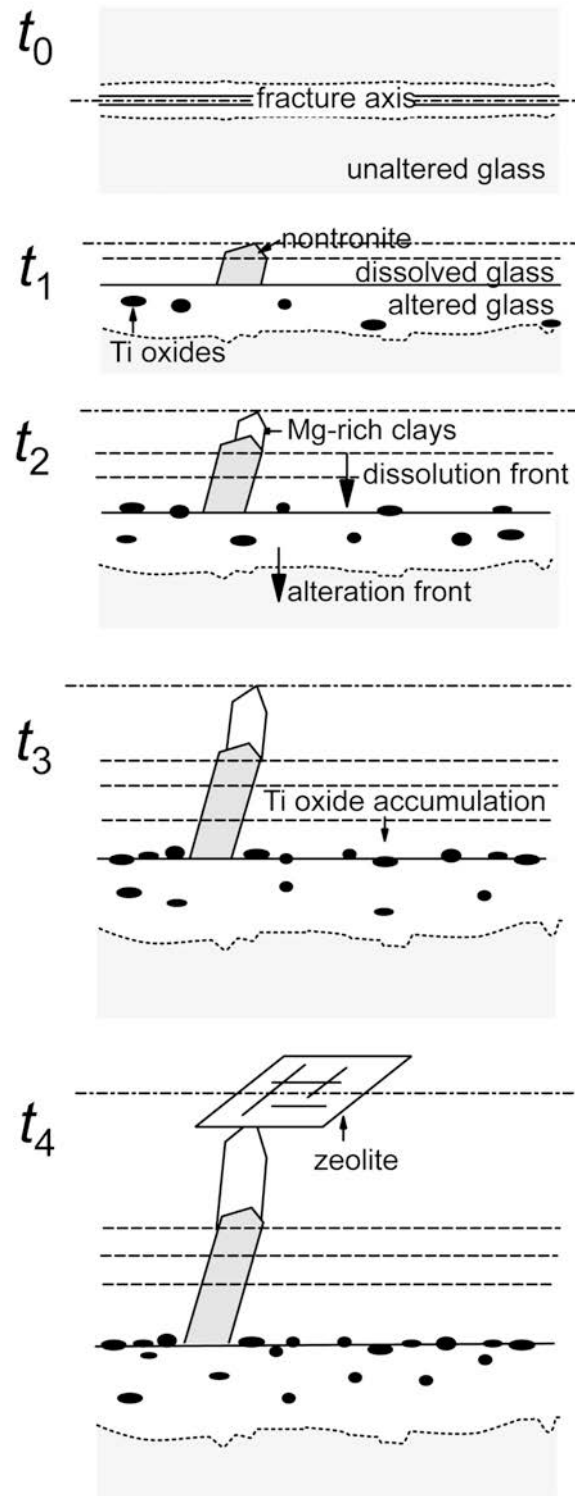


Figure 10. 10. Schematic representation of the formation of a zoned mineral deposit by alteration of a volcanic glass from a fracture. The different steps are indicated using time symbols $t_0$ to $t_x$. The alteration propagation is spatially referred to the axis of the fracture.

https://doi.org/10.1346/CCMN.2008.0560612 Published online by Cambridge University Press

(Kontak *et al.* 2002). The melt inclusions at a smaller scale confirm that the chemical composition changes progressively from basalt to trachyte with increasing crystallization (Roedder, 1979; Frezzotti, 2001). How is the value of $C_r$ estimated using petrographic analysis? $C_r$ was assumed to be estimated indirectly through the LOI values. Indeed, in the absence of amphibole and mica phenocrysts in the subaerial and submarine flows, only clay minerals and zeolites are involved in the dehydration process, triggered by the thermal treatment used to measure LOI. Clays and zeolites are located in the mesostasis (diktytaxitic voids) and the vesicles; both are classically considered to result from the alteration of a glass precursor. The greater the LOI, the lower the $C_r$. This is consistent with the mineralogical composition of the mesostasis in the subaerial and submarine flows (Mas *et al*., 2008). K-feldspar formed in the subaerial flow where $C_r$ is elevated (LOI = 1.87%). As a result, the composition of the ultimate liquid was probably trachytic. On the contrary, in the submarine flow where $C_r$ is smaller (LOI = 3.90%), no K-feldspar but pyroxene microphenocrysts were formed. According to Frezzotti (2001), the formation of pyroxene microcrysts in the diktytaxitic voids implies a weak evolution of the magma with increasing $C_r$ (andesitic residual liquid).

The presence of a glass precursor in the diktytaxitic voids signifies that the clay minerals have been formed through an alteration process. Consequently, their texture should be either randomly oriented (Banfield and Barker, 1998; Drief and Schiffman, 2004) or spherulitic-axiolitic (Lofgren, 1971a, 1971b). This is not the case in the subaerial flow where the texture of the clays is pallisadic (Figure 3d). A pallisadic texture results from the heterogeneous nucleation of minerals at the wall of the open spaces (walls of the diktytaxitic voids, crystal faces of microcrysts) and crystal growth controlled by geometrical selection (Grigor'ev, 1965). This militates for a direct precipitation from a saline solution becoming over-saturated as temperature decreased. Besides, no alteration features of plagioclase or pyroxene phenocrysts and microcrysts were observed in the vicinity of the diktytaxitic voids. The presence of skeletal K-feldspar crystals suggests that the residual liquid filling the diktytaxitic voids has experienced a brutal over-saturation with respect to K-feldspar. Skeletal crystals form by rapid growth from either highly over-saturated solutions or quenched glassy materials. In the present case, as alteration is not indicated by the petrographic data, both the skeletal K-feldspar crystals and the clay minerals were probably formed directly from a highly saline aqueous solution.

The olivine phenocrysts were completely pseudomorphosed by clay minerals and the massive inner part of the submarine flow undoubtedly experienced a late- or a post-magmatic alteration event. Thus, a glass precursor, if it existed in the diktytaxitic voids, should have been totally altered. This is supported by the randomly oriented texture of the clay matrix in which the pyroxene microcrysts are embedded (Banfield and Barker, 1998; Drief and Schiffman, 2004). However, because no glass, even andesitic, has a composition similar to pure Mg,Fe-rich clay-apatite mixtures, any alteration should necessarily induce important chemical transfers to explain the enrichment in Fe and Mg and the leaching of Si, Na, and Ca (no zeolites in the mesostasis). Such chemical transfers would have modified the crystals in contact with the connected porosity. However, no alteration features were observed in plagioclase and pyroxene microphenocrysts in the vicinity of the diktytaxitic voids (corrosion, albitization, replacement by clays). In that case, a possible alternative is that no glass precursor existed because water molecules poisoned the polymerization of silica chains (Burnham, 1979). Apatite, pyroxene, and Fe-rich clay minerals could have precipitated directly from a residual highly saline solution. This gives rise to another question: if no glass precursor was present, how did pyroxene form in the mesostasis? The synthesis experiments of Decarreau *et al.* (2004) showed that an Fe-rich aegirine crystallizes with a 2:1 phyllosilicate (ferripyrophyllite) from solutions at low-temperature conditions (200ºC) or Fe-rich smectite at higher temperatures. Thus, the hypothesis of co-precipitation of a nontronite-like clay and pyroxene from an Fe-rich residual brine during the cooling stage of the submarine flow cannot be discounted.

*Crystallization of clays from a boiling brine in the dike.* The textural relationships between euhedral microcrysts and clays in the diktytaxitic voids are different in the three basaltic bodies: they are coated by pallisadic particles in the subaerial flow; embedded in a randomly oriented matrix in the submarine flow; and coated by radially-oriented particles (muff-like) in the dike. In spite of the fact that $C_r$ is smaller for the dike (LOI = 5.69%), pyroxene did not form as expected. On the contrary, K-feldspar overgrowths are present even if less abundant than in the subaerial flow. Here, the clay minerals are the unique Fe-Mg bearing silicate phase deposited in the diktytaxitic voids. In all cases, apatite crystals formed first. However, unlike subaerial and submarine flows, the central part of all the diktytaxitic voids in the dike remained empty. This suggests a difference in the physical state of the fluid filling the diktytaxitic voids: monophase (brine) or biphase (brine + vapor) in the subaerial-submarine flows and dike, respectively. No glass precursor was formed in the dike, probably for two reasons: (1) the high concentration of water in the fluid trapped in the diktytaxitic voids increases the ionic diffusivities and favors the crystallization; (2) $H_2O$ molecules poison the formation of a glass by disrupting the Si–O–Si bonds (Burnham, 1979). Both diffusion and poisoning effects are more

https://doi.org/10.1346/CCMN.2008.0560612 Published online by Cambridge University Press

efficient as the cooling is slow. This is the case for the dike which has never been in direct contact with the atmosphere or the ocean floor. The residual liquid was over-saturated, first with respect to apatite, then, with Fe-rich clays. These conditions are encountered in boiling zones (Trommsdorff and Skippen, 1986). At the end of the crystallization process, the vapor escaped from the boiling micro-zones through zones of lower pressure in the atoll to atmosphere. Consequently, the centers of the diktytaxitic voids remained empty regardless of their size.

In summary, the glass alteration textures are similar in the quenched margins of the three basalt-hawaiite bodies. The Fe-rich clays grow inward into the glass (retreating surface) while Mg-rich clays grow outward. On the contrary, the clays filling the diktytaxitic voids (mesostasis) in the massive crystallized inner parts exhibit the following different textures according to the volcanic body. None is typical of glass alteration (Figure 11).

(1) Randomly oriented clay matrix (submarine flow) with embedded euhedral apatite and pyroxene microcrysts. The presence of a glass precursor could be supported by the textural properties but not by the chemical composition of the mesostasis.

(2) Pallisadic clays (subaerial flow) coating the walls of the open spaces (including the crystal surfaces of apatite and K-feldspar microcrysts). No glass precursor but a highly saline solution.

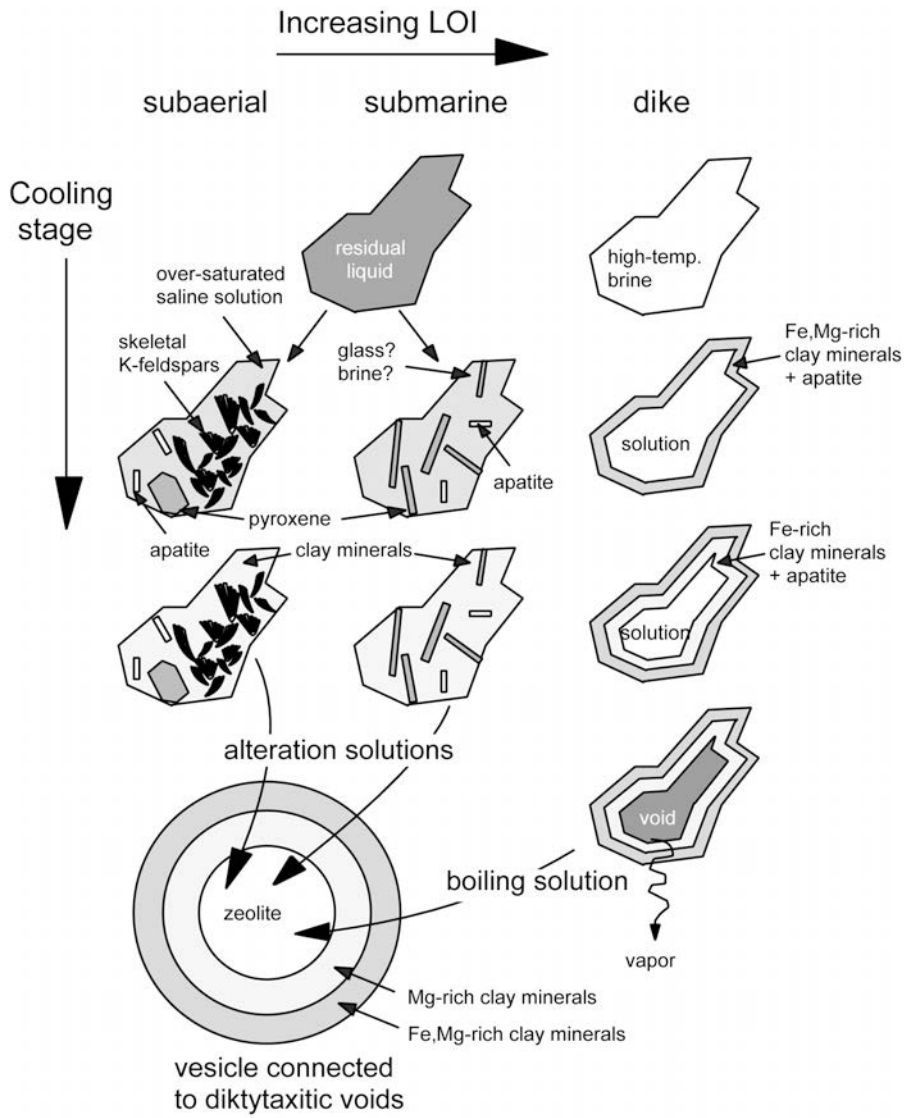


Figure 11. Schematic representation of the formation of clay minerals in the diktytaxitic voids of the subaerial and submarine flows and the dike. When present and connected to diktitaxitic voids, the vesicles are filled by a zoned mineral deposit the central part of which is zeolitic.

https://doi.org/10.1346/CCMN.2008.0560612 Published online by Cambridge University Press

(3) Clay muffs (dike) covering all the apatite needles, the central part of the void remaining empty. No glass precursor but a boiling saline solution.

*Chemical properties of the residual liquid*

*The fractionation of REE and incompatible elements.* The most incompatible elements and the *LREE* are always more concentrated in the clays filling the diktytaxitic voids than those formed in the altered chilled margins (Figures 7, 8). The amounts of *REE* in the clay fractions re-normalized to that of the corresponding inner massive part (bulk-rock composition) outline the chemical differences (Figure 12). Clays from the chilled margins of the submarine flow and the dike apparently present a distribution pattern similar to that of the massive rock (gray zone representing the average experimental error domain). Clays are slightly enriched in *REE* in the subaerial flow. On the contrary, the clay fractions from the diktytaxitic voids are significantly enriched in *REE* in the three volcanic bodies. Consequently, clay minerals from diktytitaxitic voids and chilled margins were not formed by the same process, *i.e.* alteration of a basaltic glass. The *REE* and incompatible elements are known to concentrate in the residual liquid at the end of the crystal-fractionation process (Winter, 2001). Thus, clay minerals in diktytaxitic voids could be considered to derive from the resident liquid at the end of the crystallization of the silica melt. Such a fractionation process has negligible effects in the chilled margins where the magma is quickly 'frozen' to glass.

The *LREE* distribution patterns (Figure 12) show that they are more enriched than *HREE* in the submarine and subaerial flows. This is not the case in the dike where *HREE* are even more concentrated than *LREE*. This suggests that the residual fluids have not experienced the

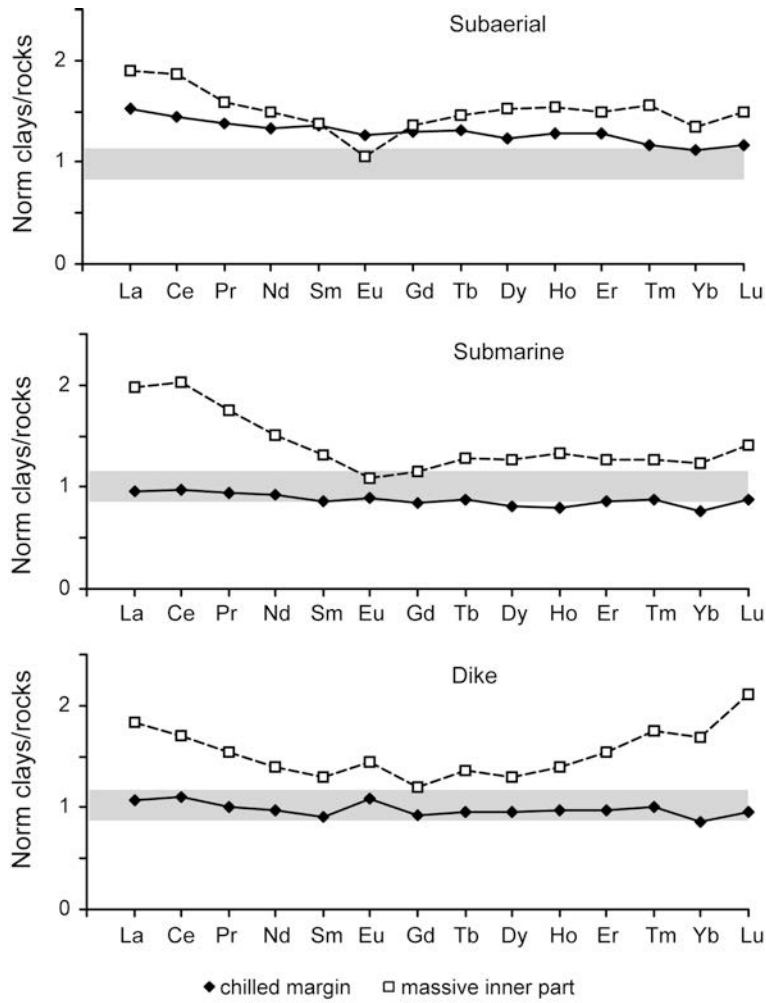


Figure 12. Amounts of *REE* normalized to the parent-rock composition of the <2 μm fraction of the chilled margins (black diamonds) and the massive inner parts (squares) of the three volcanic bodies. Gray zone: experimental error domain for the bulk-rock composition.

https://doi.org/10.1346/CCMN.2008.0560612 Published online by Cambridge University Press

same fractionation process in the three volcanic bodies. In particular, this difference suggests the presence of a separated gas phase in the dike (Greenough *et al.*, 1999). Because the textures of clays in the diktytaxitic voids do not suggest the alteration of a glass precursor, these minerals probably result from direct precipitation in a saline solution previously enriched in *LREE* and incompatible elements by the fractionation process at the end of the cooling stage.

*The Rb/Sr, $^{87}Sr/^{86}Sr$ and $^{87}Rb/^{86}Sr$ ratios*. The massive inner parts of the three volcanic bodies are richer in Sr than their corresponding chilled margins.The greater the LOI values, the greater the Rb/Sr ratio of the clay fraction (Figure 13a). Because Sr is more soluble than Rb, any water circulation should concentrate Rb in the solids (mainly clay minerals). This is typically the case for the clays in the chilled margins of the three volcanic bodies which undoubtedly result from glass alteration. In an alteration system, Rb is as much enriched in the solids as the aqueous fluid is renewed, Sr being constantly leached out of the dissolved phase. One can deduce theoretically that clays in the massive parts (mesostasis filling the diktytaxitic voids) result either from alteration with minimal renewal of fluid or from direct precipitation in the residual liquid. This is consistent with the *REE* and incompatible element fractionation.

The smaller the amount of Sr, the greater the $^{87}Rb/^{86}Sr$ ratio (Figure 13b). Clays from altered glass

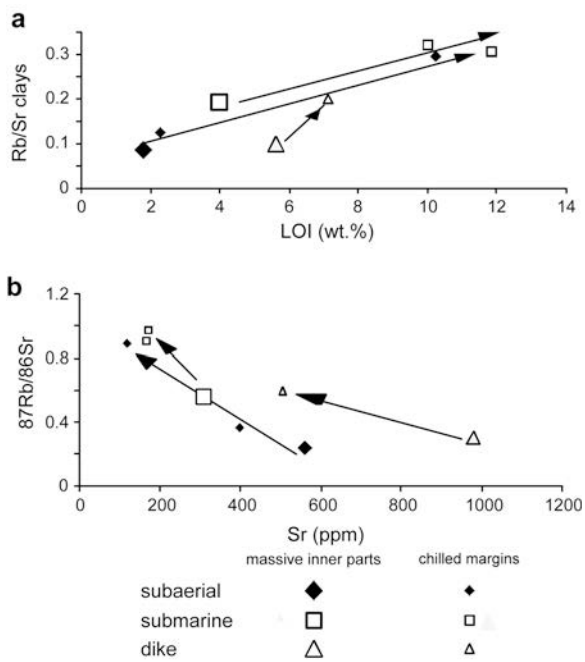


Figure 13. Amounts of Rb and Sr in the <2 μm fractions of the chilled margins and of the massive inner parts of the three volcanic bodies. (a) Rb/Sr *vs.* the loss on ignition (LOI). (b) Variation of the $^{87}Rb/^{86}Sr$ isotopic ratio *vs.* amounts of Sr.

are systematically richer in $^{87}Rb$ than clays in the diktytaxitic voids. Because clay fractions from the chilled margins and the massive parts are of the same age in each volcanic body (11.5 Ma), the means by which $^{87}Rb/^{86}Sr$ ratio varies is that the Sr ions are leached out of the altered zones. In other words, the formation of clays in chilled margins is due to the invasion of the fractures by an outer fluid (renewing solutions) while those forming the mesostasis in the massive parts should be considered to have crystallized in presence of a resident fluid.

In summary, the texture and trace-element composition indicate that the clay minerals, in spite of their rather similar crystal-chemical properties in the quenched margins and massive inner parts, did not form by the same process, *i.e.* glass alteration. The mesostasis filling the diktytaxitic voids is characterized by larger amounts of *LREE*, incompatible elements, and Sr than clays formed in the altered glass of the quenched margins.

*Origin of water and temperature conditions.* The oxygen isotopic composition of clay minerals depends on the equilibration process of the anhydrous rock with an aqueous fluid which theoretically may originate from three different sources: magmatic water; sea water, or meteoric water. For a given temperature, the equilibrium depends on the quantity of fluid involved in the formation of the clays. As the water/rock ratio was not directly measurable here, it was assumed to be proportional to LOI. Thus, a $\delta^{18}O$ *vs.* LOI plot would reflect the equilibration process in the case of two limiting conditions. Indeed, if any relationship exists between $\delta^{18}O$ and LOI, it must integrate the isotopic compositions of the non-hydrated basalt rocks, *i.e.* $\delta^{18}O$ = +5.5 to 7.0‰ for mid-ocean ridge basalt (MORB) (Taylor, 1968) and that of minerals precipitating freely from the solution. The $\delta^{18}O$ of clays irrespective of the parent rock is proportional to LOI according to a logarithmic equation (Figure 14). Using this equation, one can calculate the $\delta^{18}O$ value for clay minerals formed at low temperature from sea water: $\delta^{18}O$ = 26.5‰ (no anhydrous minerals, LOI = 100%). This calculated value is remarkably consistent with the $\delta^{18}O$ measured for Fe-rich clay minerals formed under such conditions: 26.3‰ (Buatier, 1989). The good correlation between clay $\delta^{18}O$ values and LOI indicates that sea water is the fluid to be considered in the isotopic equilibration of the clay minerals formed in both the quenched margins and the massive inner parts of the three basaltic bodies (*i.e.* no contribution by meteoric or juvenile waters). Does sea water interact with solid rocks (alteration) or magmas (contamination)? In the absence of petrological evidence for alteration, as is the case for clays in the ditytaxitic voids in the inner parts of the volcanic bodies, the sea-water component should originate from an early magma contamination. This contamination which is common in MORBs and ocean-

https://doi.org/10.1346/CCMN.2008.0560612 Published online by Cambridge University Press

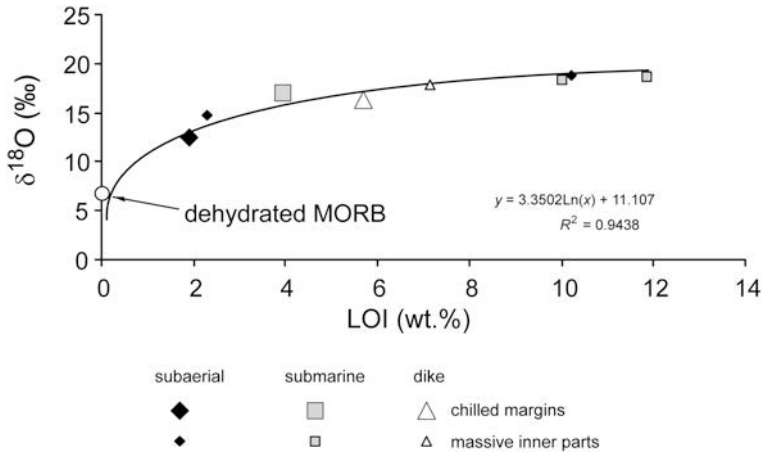


Figure 14. Relationship between the loss on ignition (LOI) and $^{18}O/^{16}O$ isotopic ratio of the clay fractions from the chilled margins and massive inner parts of the three volcanic bodies. The circle represents the $^{18}O/^{16}O$ isotopic ratio of anhydrous MORB (Taylor, 1968).

island basalts (Kent *et al.*, 1999 and references therein), results from the assimilation of sea-water-derived components by the basaltic magmas. After contamination, most of the dissolved water is expelled from the magma during the degassing process but some of it saturates the residual liquid which fills the diktytaxitic voids. If no glass precursor is formed, the newly proposed alternative is a direct crystallization of clay minerals from a residual solution which has been enriched in $H_2O$, K, P, *LREE*, and incompatible elements by a fractionation process. In such a case, clay minerals would be the last mineral species to be formed from the resident fluids which persisted in these volcanic bodies after the total crystallization of the silica melt. As they formed from direct precipitation from solutions during the cooling stage, they have to be considered as post-magmatic minerals rather than as alteration products of glass.

The isotopic geothermometer based on clay-fluid $^{18}O/^{16}O$ equilibria in alteration processes are therefore of no further use for clays filling the dyktytaxitic voids. They are pertinent only for clays formed in the altered glassy margins of the volcanic bodies. Using the equation of Savin and Lee (1988), the temperature ranges in the subaerial and submarine flows and the dike are 64−102ºC, 65−104ºC, and 71−109ºC, respectively. These temperature ranges and even higher ones, which may have prevailed in the diktytaxitic voids, are compatible with the formation of both Mg- and Fe-rich clay species: (1) Mg-rich clay minerals form from ocean-bottom temperature conditions up to 400ºC (Klopproge *et al.*, 1999, and references therein); (2) nontronite, which is classically considered as a low-temperature clay mineral, has been synthesized experimentally with Fe-rich aegirine at 200ºC (Decarreau *et al.*, 2004); (3) celadonite forms by sea-floor weathering (Pichler *et al.*, 1999) but is stable up to 410ºC (Wise and Eugster, 1964).

## CONCLUSIONS

Clay minerals present in basaltic rocks are remarkably similar, regardless of the physicochemical conditions which prevailed during their formation: nontronite, celadonite, saponite, and randomly ordered saponite-chlorite MLMs are commonly described in sea weathering, hydrothermal alteration, or diagenetic/low-grade metamorphic systems. Why are these minerals so ubiquitous? The reason could be that the parent-rock composition controls the chemistry of the active mineral systems whatever the alteration process, if the fluids are not renewed. Aluminous dioctahedral clay minerals are observed only in hydrothermal systems developed in the fractured zones around the major faults in the sea mounts (Dudoignon *et al.*, 1989). However, as shown here, clay minerals are not systematically the by-products of an alteration event. They can also be formed during a post-magmatic stage when the residual liquids are concentrated in the diktytaxitic voids. Indeed, the residual liquids are enriched in *LREE* and incompatible elements. Because they are water-saturated, they do not systematically produce an andesitic or rhyolitic glass after cooling but rather a highly saline solution which becomes over-saturated with respect to apatite and hydrous Fe-Mg bearing minerals, *i.e.* clay minerals.

Why are different textures observed in clay mineral assemblages which are otherwise so similar? Obviously, the origin of clays in basalts is not recorded in their crystal-chemical properties but rather in their texture. Their arrangement depends on the crystallization process: (1) the vein zoning results of the propagation of alteration inside the glass from an open fracture through which sea water invades the quenched margins; (2) the randomly oriented matrix in diktytaxitic voids could be due to an 'self-destruction' of the residual glass through interactions with the water saturating the residual melt (submarine flow). However, because water poisons the

https://doi.org/10.1346/CCMN.2008.0560612 Published online by Cambridge University Press

polymerization, the glass precursor may not have been formed. In that case, the clay minerals precipitated directly from the residual saline solution. This is typically the case when the texture is pallisadic (subaerial flow); (3) diktytaxitic void zoning with a free space in the center results from the explosive nucleation triggered by the boiling of the residual solutions.

*Consequences*

Because clay minerals in basalt are usually considered to be alteration by-products, the ocean composition is calculated from the chemical mass balance of sea water–basalt interactions. In other words, the greater the LOI, the greater the degree of interaction. The present study shows that clays do not necessarily form through an alteration process. The largest LOI value measured in the massive crystallized part of the three volcanic bodies is found in the dike where clays do not form through glass alteration. This should be taken into account for the calculation of the global chemical exchanges between the basalt crust and ocean water.

Another consequence concerns the exploration of Mars' surface. Indeed, the discovery of clay minerals (mainly nontronite) in some places does not automatically imply that water has been present and altered the rocks, as is commonly thought (Poulet *et al.*, 2005; Chevrier *et al.*, 2007). These clays might have been formed during the degassing stage of the lavas.

## ACKNOWLEDGMENTS

Financial support for this study was provided by the University of Poitiers (France) and the 'Institut National des Sciences de l'Univers' (INSU-CNRS). The authors are grateful to G. Giorgetti, anonymous referees, and the editorial team whose suggestions improved the manuscript.

## REFERENCES

Alt, J.C. (1999) Very low-grade hydrothermal metamorphism of basic igneous rocks. Pp. 169–201 in: *Low-grade Metamorphism* (M. Frey and D. Robinson, editors). Blackwell Science Ltd, Oxford, UK.

Anderson, A.T. Jr., Swihar G.H., Artiol G., and Geiger, C.A. (1984) Segregation vesicles, gas filter-pressing, and igneous differentiation. *Journal of Geology*, **92**, 55–72.

Andrews, A.J. (1980) Saponite and celadonite in layer 2 basalts, DSDP Leg 37. *Contributions to Mineralogy and Petrology*, **73**, 323–340.

Banfield, J.F. and Barker, W.W. (1998) Low-temperature alteration in tuffs from Yucca mountain, Nevada. *Clays and Clay Minerals*, **46**, 27–37.

Bates, R.L. and Jackson, J.A. (1987) *Glossary of Geology*. American Geological Institute, Virginia, USA, 787 pp.

Billault, V., Beaufort, D., Baronnet, A., and Lacharpagne, J.C. (2003) A nanopetrographic and textural study of grain-coating chlorites in sandstone reservoirs. *Clay Minerals*, **38**, 317–330.

Bonorino, F.G. (1959) Hydrothermal alteration in the front range mineral belt, Colorado. *Geological Society of America Bulletin*, **70**, 53–90.

Brilha, J. (1997) Cinétique de cristallisation et d'altérations post-magmatiques d'une cheminée basaltique du complexe volcanique de Lisbonne. Modélisation du refroidissement et du mécanisme de fracturation en profondeur. PhD thesis Co-tutelle, Universities of Poitiers (France) and Braga (Portugal), 177 pp.

Buatier, M. (1989) Genèse et évolution des argiles vertes hydrothermales océaniques. Les 'Monts' du rift des Galapagos (Pacifique Equatorial). PhD thesis, University of Strasbourg (France), 175 pp.

Burnham, C.W. (1979) The importance of volatile constituents. Pp 439–482 in: *The Evolution of Igneous Rocks, Fiftieth Anniversary Perspectives* (H.S. Yoder Jr, editor). Princeton University Press, New Jersey.

Chevrier, V., Poulet, F., and Bibring, J.P. (2007) Early geochemical environment of Mars as determined from thermodynamics of phyllosilicates. *Nature*, **448**, 60–63.

Decarreau, A., Petit, S., Vieillard, P., and Dabert, N. (2004) Hydrothermal synthesis of aegirine at 200ºC. *European Journal of Mineralogy*, **16**, 85–90.

DeGraff, J.M. and Aydin, A. (1993) Effect of thermal regime on growth increment and spacing of contraction joints in basaltic lava. J*ournal of Geophysical Research*, **98**, 6411–6430.

DePaolo, D.J. (1986) Detailed record of the Neogene Sr isotopic evolution of seawater from DSDP Site 590B. *Geology*, **14**, 103–106.

Destrigneville, C., Schott, J., Caristan, Y., and Agrinier, P. (1991) Evidence of an early alteration process driven by magmatic fluids in Mururoa volcano. *Earth and Planetary Science Letters*, **104**, 119–139.

Drief, A. and Schiffman, P. (2004) Very low temperature alteration of sideromelane in hyaloclastites and hyalotuffs from Kilauea and Mauna Kea volcanoes: implications for the mechanism of palagonite formation. *Clays and Clay Minerals*, **52**, 622–634.

Dudoignon, P., Meunier, A., Beaufort, D., Gachon, A., and Buigues, D. (1989) Hydrothermal alteration at Mururoa Atoll (French Polynesia). *Chemical Geology*, **76**, 385–401.

Dudoignon, P., Proust, D., and Gachon, A. (1997) Hydrothermal alteration associated with rift zones at Fangatauffa atoll (French Polynesia). *Bulletin of Volcanology*, **58**, 583–596.

Eggleton, R.A. and Keller, J. (1982) The palagonitization of limburgite glass – A TEM study. *Neues Jahrbuch für Mineralogie Monatshefte*, **H7**, 321–336.

Frezzotti, M.L. (2001) Silicate-melt inclusions in magmatic rocks: application to petrology. *Lithos*, **55**, 273–299.

Goff, F. (1996) Vesicle cylinders in vapour-differentiated basalt flows. *Journal of Volcanology and Geothermal Research*, **71**, 167–185.

Greenough, J.D., Lee, C.Y., and Fryer, B.J. (1999) Evidence for volatile-influenced differentiation in a layered alkali basalt flow, Penghu Islands, Taiwan. *Bulletin of Volcanology*, **60**, 412–424.

Grigor'ev, D.P. (1965) *Ontology of Minerals*. Israel program for scientific transactions Ltd, S. Marson, Jerusalem, 250 pp.

Guille, G., Goutiere, G., and Sornein, J.F. (1993) *Les atolls de Mururoa et Fangataufa (Polynésie Française). 1 – géologie, pétrologie, hydrogéologie (édification et évolution des édifices).* Monographie DIRCEN/CEA, Masson, Paris.

Jaeger, J.C. (1968) Cooling and solidification of igneous rocks. Pp. 503–536 in: *Basalts: the Poldervaart Treatise on Rocks of Basaltic Composition*, vol. **2**, Wiley & Sons, Chichester, UK.

Kent, A.J.R., Clague, D.A., Hunda, M., Stolper, E.M., Hutcheon, I.D., and Norman, M.D. (1999) Widespread assimilation of a seawater-derived component at Loihi Seamount, Hawaii. *Geochimica et Cosmochimica Acta*, **63**, 2749–2761.

Kloprogge, J.T., Komarneni, S., and Amonette, J.E. (1999) Synthesis of smectite clay minerals: a critical review. *Clays and Clay Minerals*, **47**, 529–554.

Kontak, D.J., De Wolfe deYoung, M.Y, and Dostal, J. (2002) Late-stage crystallization history of the Jurassic North Mountain basalt, Nova Scotia, Canada. I. Textural and chemical evidence for pervasive development of silica-liquid immiscibility. *The Canadian Mineralogist*, **40**, 1287–1311.

Lofgren, G. (1971a) Experimentally produced devitrification textures in natural rhyolitic glass. *Geological Society of America Bulletin*, **82**, 111–124.

Lofgren, G. (1971b) Spherulitic textures in glassy and crystalline rocks. *Journal of Geophysical Research*, **76**, 5635–5648.

Mas, A., Meunier A., Beaufort, D., Patrier, P., and Dudoignon, P. (2008) Clay minerals in basalt-hawaiite rocks from Mururoa atoll (French Polynesia). I. Mineralogy. *Clays and Clay Minerals*, **56**, 711–729.

Maury, R.C., Caroff, M., Achard, S., Guille, G., Joron, J.L., Gachon, A., Rocaboy, A., and Leterrier, J. (1992) L'atoll de Mururoa (Polynésie Française). La série magmatique. *Bulletin de la Société Géologique de France*, **163**, 659–679.

McPhie, J., Doyle, M., and Allen, R. (1993) Volcanic textures, a guide to the interpretation of the textures in volcanic rocks. Pp. 21–71 in: *CODES Key Centre*, University of Tasmania.

Meunier, A. (1994) Mechanism of fluid palaeocirculations in fractured rocks determined by vein alteration studies. Pp. 365–378 in: *Hydrocarbon and Petroleum Geology of France* (A. Mascle, editor), Springer-Verlag, Berlin.

Pichler, T., Ridley, W.I., and Nelson, E.P. (1999) Low-temperature alteration of dredged volcanics from the Southern Chile ridge: additional information about early stages of seafloor weathering. *Marine Geology*, **159**, 272–285.

Pouchou, J.L. and Pichoir, F. (1984) A new model for quantitative analysis. I. Application to the analysis of homogeneous samples. *La Recherche Aérospatiale*, **3**, 13–38.

Poulet, F., Bibring, J.P, Mustard, J.F., Gendrin, A., Mangold, N., Langevin, Y., Arvidson, R.E., Gondet, B., Gomez, C., and the Omega Team (2005) Phyllosilicates on Mars and implications for early Martian climate. *Nature*, **438**, 623–627.

Reed, S.J.B. (1993) *Electron Probe Microanalysis*, 2nd edition. Cambridge University Press, Cambridge, UK.

Roedder, E. (1979) Origin and significance of magmatic inclusions. *Bulletin de Minéralogie*, **102**, 487–510.

Ryan, M.P. and Sammis, C.G. (1981) The glass transition in basalt. *Journal of Geophysical Research*, **86**, **B10**, 9519–9535.

Savin, S.M. and Lee, M. (1988) Isotopic studies of phyllosilicates. Pp. 189–223 in: *Hydrous Phyllosilicates (Exclusive of Micas)* (S.W. Bailey, editor). Reviews in Mineralogy, **19**, Mineralogical Society of America, Washington, D.C.

Schiffman, P. and Day, H.W. (1999) Petrological methods for the study of very low-grade metabasites. Pp 108–142 in: *Low-grade Metamorphism* (M. Frey and D. Robinson, editors), Blackwell Scientific Ltd, Oxford.

Staudigel, H. and Hart, S.R. (1983) Alteration of basaltic glass: Mechanism and significance of the oceanic crust-sea water budget. *Geochimica et Cosmochimica Acta*, **47**, 337–350.

Sun, S.S. and McDonough, W.F. (1989) Chemical and isotopic systematics of oceanic basalts: implications for mantle composition and processes. Pp. 313–345 in: *Magmatism in the Ocean Basins* (A.D. Sanders and M.J. Norry, editors). Blackwell Scientific Publishers, Oxford.

Taylor, H.P. Jr (1968) The oxygen isotope geochemistry of igneous rocks. *Contributions to Mineralogy and Petrology*, **19**, 1–71.

Thorseth, I.H., Furnes, H., and Tumyr, O. (1991) A textural and chemical study of Icelandic palagonite of varied composition and its bearing on the mechanism of glass-palagonite transformation. *Geochemica et Cosmochimica Acta*, **55**, 731–749.

Trommsdorff, V. and Skuppen, G. (1986) Vapour loss ('boiling') as a mechanism for fluid evolution in metamorphic rocks. *Contributions to Mineralogy and Petrology*, **94**, 317–322.

Veizer, J. (1989) Strontium isotopes in seawater through time. *Annual Review of Earth and Planetary Sciences*, **17**, 141–167.

Walker, G.P.L. (1989) Spongy pahoehoe in Hawaii: a study of vesicle distribution patterns in basalt and their significance. *Bulletin of Volcanology*, **51**, 199–209.

Winter, J.D. (2001) *An Introduction to Igneous and Metamorphic Petrology*. Prentice Hall, New Jersey, 699 pp.

Wise, W.S. and Eugster, H.P. (1964) Celadonite: synthesis, thermal stability and occurrence. *American Mineralogist*, **49**, 1031–1083.

Zhou, Z. and Fyfe, W.S. (1989) Palagonitization of basaltic glass from DSDP Site 335, Leg 37: Textures, chemical composition, and mechanism of formation. *American Mineralogist*, **74**, 1045–1053.

(*Received 8 April 2008; revised 12 September 2008; Ms. 0152; A.E. W. Huff*)